Lloyd, Eric, M.S. December 2023 EARTH SCIENCES

HOW SEDIMENT SIZE HETEROGENEITY CONTROLS THE PIPIING POTENTIAL: A LABORATORY STUDY

Thesis Advisor: Dr. Kuldeep Singh

ABSTRACT

Piping or internal erosion has been responsible for almost half of all dam failures worldwide. In this research, we studied the influence of grain size heterogeneity, as characterized by sediment size (d_{50}) and the uniformity coefficient (C_u), on piping potential. A novel experimental setup was designed in-house that included sediment mass, pressure, and turbidity sensors allowing the examination of transient changes during piping events. Porosity and conductivity were analyzed in order to compare trends across varying grain size distributions. Mass values of soil lost during piping failure via a continuous mass balance and a turbidity meter to capture fines that remain in suspension were both utilized to capture the magnitude of piping failure. Minute Piping and Clogging events that are only able to be captured via the pressure transducers were recorded during this experiment, adding complexity to the onset of piping phenomena. The smaller the C_u, the less clogging events occurred before piping failure. It was noted that these minute piping and clogging events would stabilize as the sediment column reached equilibrium. This research allows for further studies to expand on these piping and clogging events as well as depicted trends between soil heterogeneity and piping potential.

HOW SEDIMENT SIZE HETEROGENEITY CONTROLS THE PIPIING POTENTIAL: A LABORATORY STUDY

A thesis submitted

to Kent State University in partial

Fulfilment of the requirements for the

Degree of Master of Science

By

Eric C. Lloyd

December 2023

Thesis written by

Eric Christopher Lloyd

B.S. Youngstown State University, 2020

M.S. Kent State University, 2023

Approved by

Kuldeep Singh _____, Advisor

Daniel K. Holm _____, Chair, Department of Earth Sciences

Mandy Munro-Stasiuk _____, Dean, College of Arts and Sciences

TABLE OF CONTENTS

LIST OF FIGURES

1.0 Introduction

1.1 Significance and Previous Research

Piping is defined as internal erosion and creation of voids within soils due to seepage of water through pore spaces that dislodges fine particles without destroying the structure of the soil (Indraratna et al., 2011). Piping is referred to by several other names such as suffusion, subterranean erosion, and sinkhole erosion (Bernatek-Jakiel & Poesen, 2018). Piping is not a new concept and has been studied in detail, as Karl von Terzaghi was the pioneer in describing piping occurring at a critical head value that became the basis of the theory of the critical hydraulic gradient (Terzaghi, 1939). Following his research, piping has been studied with focus on compactness, stress states, and constant gradients (Chang & Zhang, 2013; Liang et al., 2017; Luo et al., 2013; Richards & Reddy, 2010; Skempton & Brogan, 1994).

Figure 1. Field Experiment of Piping (Wilson et al., 2013) depicting the magnitude of piping failure.

This phenomenon is particularly important in areas affected by glaciers due to the glacial outwash that the subsurface is composed of. Dams built in these areas are underlain by silt and sand lens that are highly susceptible to piping. If piping occurs in the sands or silts located under the foundation of a dam, the dam may become structurally damaged and fail.

Figure 1 shows a field experiment illustrating the progression of a piping failure. The experiment was conducted by the United States Department of Agriculture-Agriculture Research Service (USDA-ARS) laboratory in Stillwater, Oklahoma. As one can see, it took only 60 minutes for a complete failure of the structure (Wilson et al., 2013). This reveals the dangers of constructing hydraulic barriers without accounting for the possibility of a piping failure.

"Strength Reduction of Cohesionless Soil Due to Internal Erosion Induced by One-Dimensional Upward Seepage Flow" by Ke and Takahashi, 2014, provides valuable information. Ke and Takahashi clarify that piping occurs in media that contain larger voids throughout, such as gap-graded soils. This is well known, but the paper goes onto explaining how this loss of material can affect the strength of the soil in natural and engineered structures as well as depict a substantial increase in hydraulic conductivity. Regarding soil strength, Ke and Takahashi explain that as a soil undergoes piping, the fines within the soil matrix are removed, leaving behind a coarser skeleton of the soil. This soil skeleton consisting of little to no fine-grained sediments can be unstable and prone to failure. Fine-grained sediments being present in a soil matrix allow for the larger sediments to be secured into place by removing the large pore spaces, thus leaving little room for shifting of sediments to occur. Allowing shifting of sediments by removing fines can lead to failure to structures constructed on the soil that has been affected by piping phenomena. Regarding increase in hydraulic conductivity, piping creates voids that water flows through within a soil matrix. Allowing these voids gives a less tortuous path for flow to take place and allows for faster flow of water through the soil. Ke and Takahashi noted that a relationship follows Darcy's Law and was linear when comparing the average hydraulic gradient to permeability. After piping occurs, this relationship is no longer linear as the hydraulic conductivity drastically increases (Ke & Takahashi, 2014).

These studies provide valuable information on the piping phenomena, but a knowledge gap is present in the study of sediment size heterogeneity as a function of time when piping occurs. Studying how the time at which piping occurs versus the alteration of the coefficient of uniformity while keeping the d_{50} of the soil constant would provide insight on how altering the gradation effects the timing of which structural failure of a soil begins.

As Terzaghi and others have stated, the critical hydraulic gradient is accepted to be a large control on piping (ALsakran et al., 2021; Israr et al., 2019; Tian et al., 2020; Zhang et al., 2020). The rule that piping failure can occur as the hydraulic gradient averages one was noted by Holtz and Kovacs (Holtz et al., 2011). Upon further research, Nguyen and Plé, 2013, determined that piping can in fact occur with gradients less than 1 (Nguyen et al., 2013). This is crucial as often in mountainous terrain, gap-graded soils from the same region are used as subgrade filling material due to the difficulty of transporting large amounts of filling material from other locations. Gap-graded systems are very susceptance to piping at low gradients so considering that piping can occur below a gradient of one is crucial in this instance (Zhang et al., 2020).

These findings prove to be valuable to the understanding of how piping develops and occurs, but a research gap lies in studying all aspects of the control that sediment size and heterogeneity play on piping phenomenon. Research has been done by D. S. Chang, A. and L. M. Zhang, 2013, regarding critical hydraulic gradients in their paper “Critical Hydraulic Gradients of Internal Erosion under Complex Stress States” published in 2013. Upon review of the research conducted by Chang and Zhang, it was noted that there are four distinct phases during piping failure. The four phases can be associated with the stable condition of the soil, the initiation of piping, the development of piping, and the failure due to piping. During the stable stage, the mass is constant and there is no visible erosion. During the initiation of piping, the mass slightly

increases as there is a small loss of fines while the soil still retains its integrity. During the developmental stage of piping, soil can be seen migrating from the sample, there is a large increase in mass recorded, and the soil sample becomes deformed. The final stage, the failure due to piping, depicts shear failure due to piping and total deformation of the sample has occurred. Along with these four stages, three alterations in permeability were noted. These three alterations can be defined from the piping initiation, skeletal deformation, and total failure aspects of piping. These permeability changes are correlated with the loss of fines within the sample. Chang and Zhang have graphically shown the loss of fines by relating the loss of fines by weight to the duration the experiment was conducted at. This can be seen in figure 2 (Chang & Zhang, 2013). This is high quality research that studies mass and permeability but fails to capture the loss of fines that may become suspended within the affluent water. In order to completely study all aspects of piping, these fines must not be excluded from being recorded.

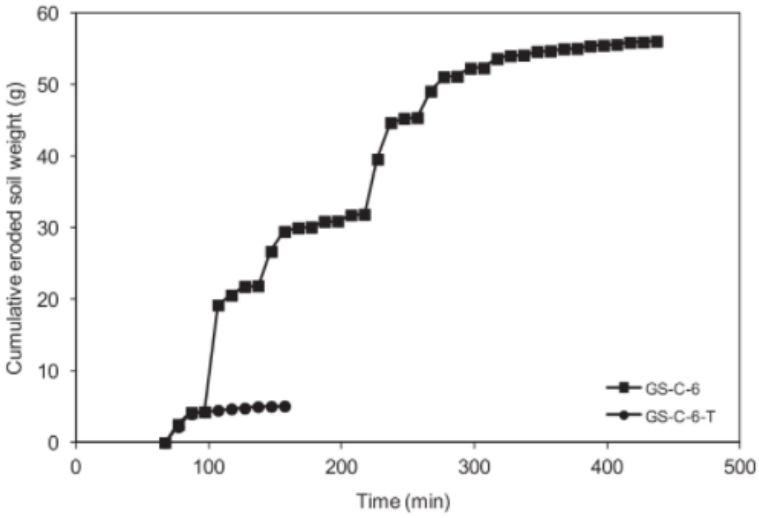

Figure 2. Plot of Eroded Soil by Weight (Chang & Zhang, 2013) depicting numerous stages of piping failure and the mass lost during each stage.

Mohamad Oueidat, 2021, captures this study of suspended fines in his research Effect of Fine Particles and Soil Heterogeneity on the Initiation of Suffusion. Ouiedat captures these fines via the metric of turbidity and depicts piping events via a graph showing a spike in turbidity values as seen in figure 3. There are also comparisons to flow rate and head loss, which is valuable when analyzing the different metrics together. However, there lies a research gap in

regard to piping where the sediment sizes these experiments are conducted on as well as data lacking. The soils tested all have Uniformity Coefficient values less than 3, which creates a need for research on soils that are well graded. The uniformity coefficient (C_u) is calculated from a sediment distribution following $C_u=d_{60}\backslash d_{10}$. Where d_{60} is the value for 60% of the grain sizes existing within the sample and d_{10} is the value for where 10% of the grain sizes exist within the

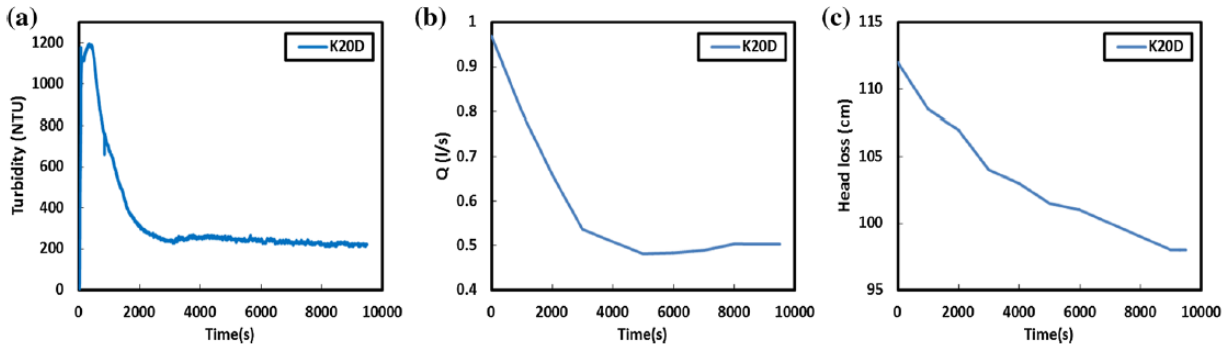

Figure 3. Experimentation done by Ouiedat et al. in 2021 depicting the decrease of flow rates (subgraph b) using the two metrics of turbidity (subgraph a) and head loss (subgraph c). Only soils with Uniformity Coefficients less than 3 were used during this experimentation.

sample. The graphs also only provide data decreasing the flow rate. Data is needed on if the rate of flow is increased to understand piping. Mass lost is included in this experiment as well, but as there is no indication that the flow rate was increased, thus increasing the head gradient, further expansion on this research is needed(Oueidat et al., 2021).

A laboratory study capturing all aspects of piping can significantly improve the knowledge about the role of grain size distribution and sediment size in piping potential compared to a study done in the field due to the greater ability to control the variables involved. Using differing bins of grain sizes to create a soil mixture of a desired distribution allows for clear study of this factor alone on a soil's ability to pipe. Having the ability to alter the hydraulic gradient while keeping the grain size distribution constant is a benefit that is unable to be obtained in the field. The effect of grain size distribution on piping potential of a soil can also help better understand processes like gulley erosion and landslides where piping can be a

dominant mechanism (Wilson, et al., 2020). By understanding the process that is the foundation to these mass wasting events, a better understanding of how to prevent and remediate such events can be researched.

There lies a knowledge gap in the aspect of relating the composition of soils in regard to weight of differing grain sizes in a sample compared to the ability of a soil to pipe. The benefit of this laboratory study is that this can be controlled and investigated. Soil samples can be created by mixing certain weights from differing grain sizes. The ratio of these weights can be used as an index to demonstrate heterogeneity within the soil sample that has been created. This can then be related to the permeability and porosity of the soil during piping failure.

1.2 Theory of piping

There are several factors that contribute to the ability of soil to pipe. One of the most critical among these is the hydraulic gradient. It is well known that piping can occur when hydraulic head is greater than the seepage path. In loose sands and silts, piping can occur when the hydraulic gradient is equal to 1 (Holtz et al., 2011; (Atallah et al., 2013)).

Another important aspect of soil piping is the type of soil. Cohesive soils, such as clays, do not pipe. The greater the cohesion of the soil, the less likely is the soil to pipe. Shown in Figure 4 is a soil matrix that contains fine-grained cohesive material (Grabowski et al., 2011). The pore spaces between the silt and sand size particles are filled with clay particles that have a higher amount of cohesion than that

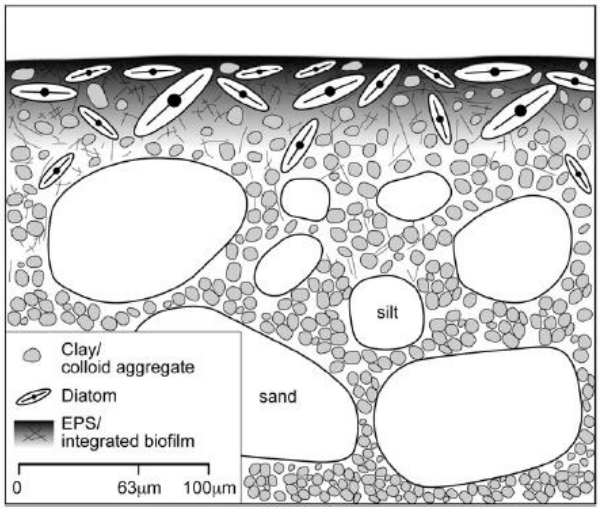

Figure 4. Soil matrix containing cohesive fines shown by Grabowski et al. in 2011 that is more resistant to piping failure due to the inclusion of the cohesive fines

of silt and sands. A soil that shows these characteristics is less likely to pipe than soils without cohesive fines. Similarly, coarse sands and gravels do not pipe because individual particles are too heavy to be removed by the seepage forces. According to Ke & Takahashi, 2012, in order for piping to occur, the fine sediment in a soil must be smaller than the pore spaces of the larger particles. If this criterion is not met, the seepage flow will not be able to dislodge the fines in order to initiate piping.

Finally, the relative density (actual density/maximum dry density) of a soil can influence its piping potential. As density of a soil increases, its piping potential decreases. As a soil becomes more dense, angular grains in a soil can interlock and become stable, preventing the removal of the grains via piping. A soil that is less dense does not convey the interlocking grains, thus creating a media that more readily pipes. This idea can be correlated to the C_u of a soil. The C_u values represent whether a soil sample is well-sorted, poorly graded, or poorly sorted or well graded. For example, C_u >15 indicates the soil is well-graded. The soil is poorly graded if the C_u value ranges from 2-3. If the C_u is ~ 1, the soil is well-sorted (Holtz & Kovacs, 1981). Increasing the C_u also increases the density, as pore spaces are removed and replaced by sediment particles. Thus, an increase in Cu decreases a soil's ability to pipe.

1.3 Research Needs

In order to fill this gap in research, a study is conducted to capture and study in depth the hydraulic gradient, the mass of sediment lost, and the turbidity during a piping event. This will not only fill the gap in research but also tie together previous research by combining certain aspects of work done prior to this study. To conduct this research successfully, the question of what the effect of heterogeneity on piping potential needs to be kept in mind during experimentation.

Based on previous research, the hypothesis for the research is that the larger the C_u of a sediment mixture is, the greater the hydraulic gradient needed to initiate piping will need to be. A secondary hypothesis is as the grain size distribution of a sandy or silty soil decreases, the potential for failure via piping increases. In order to test these hypotheses and fill the knowledge gap, a laboratory study is conducted to obtain and analyze high quality data. The experimentation process is unique as it cross-references hydraulic gradient, mass extruded, and affluent turbidity to gain a better understanding of how these metrics depict piping phenomena within soil mixtures of differing heterogeneity.

2.0 Methods

2.1 Soil Selection

We investigate the piping phenomenon of soils using a set of sediment sizes and sediment grades. First, we synthesis well-sorted sediments of three different d_{50} sizes. The d_{50} value depicts the median sediment size of a sediment distribution. Then, each of the d_{50} categories forms the basis for a set of three differently graded sediments resulting in a total of nine soils investigated in this study. The three d_{50} sediment sizes include, 1mm, 0.7mm, and 0. 3mm (Holtz & Kovacs, 1981). For each d_{50} size, we synthesize three sediment grades quantified using C_u.

In this study, we used three average Cu of 6.5, 3, and 1.5 to synthesize soils representing three significantly different sediment grades allowing testing a large scope of soils.

It is known that fine sands and silts are susceptible to piping (Atallah, 2013). Piping includes the loss of fine sediments within a soil matrix due to the preferential seepage of water. We begin out study by isolating sediments into thirteen bins of sand and one bin of silt by employing the mechanical sieving methods. The mechanical sieving isolates sediment sizes

based on sieve sizes following American Society for Testing and Materials (ASTM) standards, summarized in Table 1.

Table 1. Soil Bin Sizes and Classifications

Medium Pebbles	7/16” sieve (11.3mm) to 3/8” sieve (9.52mm)
Fine Pebbles	5/16” sieve (8 mm) to 0.265” sieve (6.73 mm)
Very Fine Pebbles	#5 sieve (4 mm) to #6 sieve (3.36 mm)
Very Coarse Sand	#10 sieve (2mm) to #14 sieve (1.41mm)
Very Coarse Sand	#14 sieve (1.41mm) to #18 sieve (1mm)
Coarse Sand	#18 sieve (1mm) to #25 sieve (0.707mm)
Coarse Sand	#25 sieve (0.707mm) to #35 sieve (0.5mm)
Medium Sand	#35 sieve (0.5mm) to #45 sieve (0.354mm)
Medium Sand	#45 sieve (0.354mm) to # 60 sieve (0.25mm)
Fine Sand	#60 sieve (0.25mm) to #80 sieve (0.177mm)
Fine Sand	#80 sieve (0.177mm) to #120 sieve (0.125mm)
Very Fine Sand	#120 sieve (0.125mm) to #170 sieve (0.088mm)
Very Fine Sand	#170 sieve (0.088mm) to #200 sieve (0.074mm)
Silt	<#200 sieve (0.074mm)

These 14 bins of unique sediment sizes are used to create the nine differing mixtures of soil. Based on the soil desired to be tested, different amounts of these soils are mixed to create samples that are subject to piping tests to better understand their behavior when piping conditions are applied. The grain size distribution test is performed on the created samples, following the American Society for Testing and Materials (ASTM) method C-136 (ASTM, 2010) as well as via the Camsizer at Kent State University. The data is used to plot the grain size distribution curves of the samples created from the 14 bins of differing grain sizes. These bins of sediment are created according to the American Society for Testing Materials (ASTM) classification system. Using the ASTM classification system, a medium pebble is defined as having a particle size ranging from 16mm to 8mm, a fine pebble ranges from 8mm to 4mm, a very fine pebble ranges from 4mm to 2mm, a very coarse sand ranges from 2mm to 1mm, a coarse sand ranges from 1mm to 0.5mm, a medium sand ranges from 0.5mm to 0.25mm, a fine sand ranges from 0.25mm to 0.125mm, a very fine sand ranges from 0.125mm to 0.062mm, and

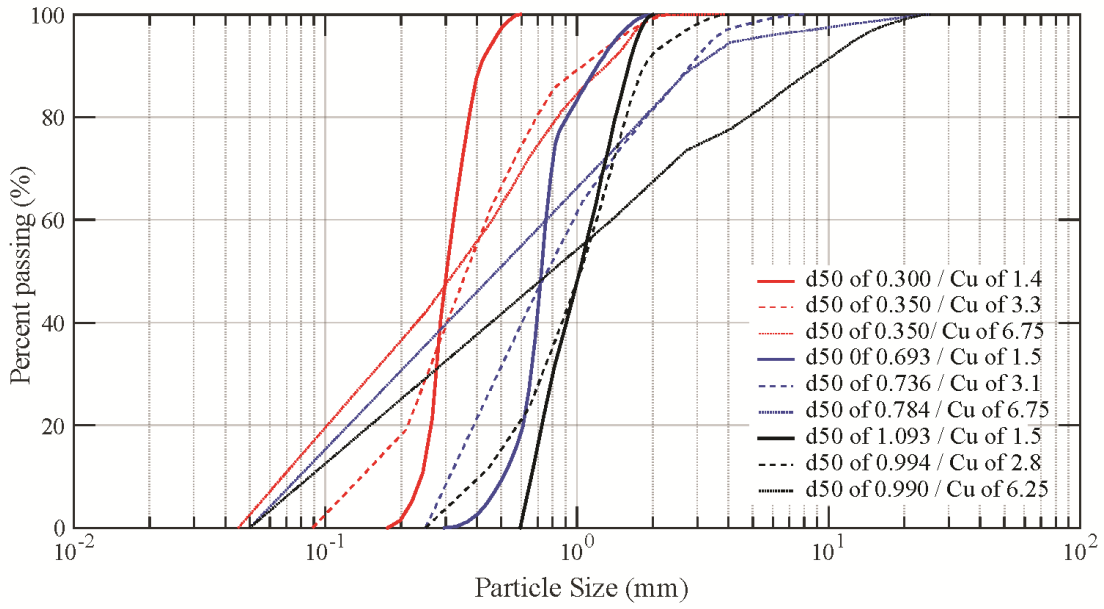

Figure 5. Sediment size distributions created for this study depicting a wide range of soil types that were subject to piping conditions.

a silt can be classified as any sediment smaller than 0.062mm (ASTM, 2010). Using these bins, the nine-sediment grain size distribution (GSD) curves are created and can be seen in figure 5.

The sediment inserted into the column was mixed via the use of a sediment splitter apparatus. The sediment splitter was used three differing times on a given mixture of soil prior to insertion into the sediment column to remove as much human error during sediment creation as possible. The mixed sediment was then inserted via a large funnel to prevent spilling. The funnel outlet was large in diameter in order to prevent unnatural clogging of sediment as it was poured into the column. After the sediment is poured into the column, the column is vibrated via a shaker table until sediment cannot be further condensed with vibrations. The column is then again filled with sediment to remove any voids created by the vibrating process with sediment and ready for experimentation. The sediment column is described in detail in section 2.4.

2.2 Experimental Setup

An experimental apparatus was created to thoroughly investigate piping phenomena. The setup design can be seen in figure 6.

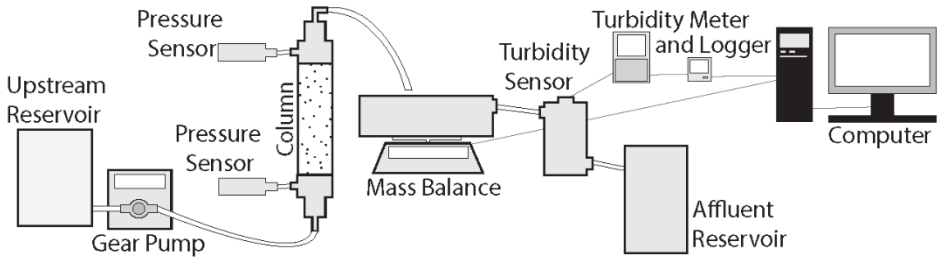

Figure 6. Experimental setup schematic that was created to design the testing apparatus.

As seen in figure 6, an upstream reservoir is used to create a constant supply of water to the gear pump. The gear pump allows for a constant and smooth flow for the piping column experiments. The column inlet has a filter placed on the bottom to allow for flow to enter

uninhibited while preventing soil from falling down into the tube connecting to the gear pump. This filter has an aperture of 0.595mm. This size filter was found best suited to prevent sediment from clogging the gear pump while allowing for even flow to occur. The top of the column does not have a filter to allow for the piping phenomena to occur. Attached to the column are two pressure transducers connected at differing elevations, which data log via Bluetooth communication between the sensors and the computer. Using pressure drop between these sensors, the hydraulic head of the column of sediment is calculated. Sediments expelled from the column due to piping are recorded via the mass balance, which data logs to the computer. In this step, a reservoir is placed on the balance with overflow protection in place. This allows for constant mass of water to be recorded. By noting this constant mass, and mass increase allows estimation of soil mass expelled. The fine sediments expelled cannot not be accurately captured via the mass balance due to their small diameter keeping them in suspension which transport downstream to the effluent reservoir. In evaluating these fine sediments, a turbidity sensor is

Figure 7. Final experimental setup design used to conduct piping experiments

installed in between the overflow protection of the mass balance and the downstream effluent reservoir. The suspended fine particles that are expelled from the sample would pass through the turbidity sensor allowing for these sediments to be used as an index of piping. The turbidity sensor also records the turbidity values in real time, allowing for comparison of these values against the mass and pressure values recorded. Once the water exists the turbidity sensor, the water is collected in an affluent reservoir and deposited appropriately. Image 7 depicts the constructed setup built to design of figure 6.

2.3 Gear Pump

The gear pump used is a Lead Fluid model CT30000F. The pump is a magnetic drive pump that does not include pulsations, for example, found from peristaltic pump and instead allows for a constant smooth velocity. The flow rate of this pump ranges from 15mL/min to 2700mL/min. An image of the gear pump can be seen in image 8. The use of this pump allows for a consistent adjustment of flow rate to obtain the desired hydraulic gradient which is monitored live via pressure sensors.

Figure 8. Leadfluid Gear Pump used for experimentation that allowed for a constant, controlled flow rate.

2.4 Sediment Column

The sediment column is constructed from a 2.24inch in diameter plexiglass tube that is 12 inches in length. There is a filter placed on the bottom of the column to prevent sediment from falling out of the column into the tube connected to the gear pump. This filter is mesh of an aperture of 0.595mm, or in correlation with a #30 ASTM mesh. The bottom of the column was glued with epoxy resin to prevent any leaking from pressure induced during the piping test.

Figure 9. Sediment Column allowing for upward seepage flow. The column contains a filter with an aperture of 0.595mm on the bottom to prevent sediment returning into the tubing. No filter is present at the top of the column to allow for piping to occur.

The top of the column is removable to allow sediment to be inserted. In order to prevent leaks, Teflon plumbers' tape was used to remove any gaps within the threads of the column. No mesh was placed on the top of the sediment as piping would not occur with a filter in place. Two holes were drilled in the side of the column to allow for the pressure transducers to be attached. Plastic nipples were put in place and epoxy was used to prevent any leaks. A fine mesh of 0.125mm, in correlation with a #120 ASTM mesh, was used to prevent sediment from clogging the plastic nipples and altering the pressure transducers accuracy. To further prevent leaks, a clamp was placed on the tube entering the column to prevent detachment when high pressure systems were created. An image of the sediment column can be seen in image 9.

2.5 Pressure Sensors

The pressure sensors used are Pasco wireless pressure sensors PS-3203. These sensors have a range capable of capturing pressure values from 0-400kPa. The resolution is 0.1kPa and an accuracy of ±2kPa. These sensors are equipped with Bluetooth capabilities to allow for ease of recording changes in pressure of the sample. These pressure sensors used were capturing data points at a frequency of one data point per second. This high frequency allows for high resolution of hydraulic behavior within the sample. This high resolution allows for the capture of minute piping and clogging events. These minute events are described in greater detail in the results section. Using two of these pressure sensors, calculations can be made to convert the change in pressure between the two sensors to the hydraulic gradient (i) following, $i = dP/\rho gL$, where P is pressure in Pascals, dP is pressure difference from the two Pasco wireless sensors, g is acceleration due to gravity, and L is column length between the two sensors.

The use of these equations allows for manual increase in pressure to consequently increase the hydraulic head, thus allowing for an accurate study of the threshold for piping to occur at a given hydraulic head. To accurately record this, the pressure sensors are attached and zeroed at the same elevation in relation to the sediment column where the sensor is recording from. This removes any error that atmospheric pressure may cause. The sensors used are depicted in image 10.

Figure 10. Pasco Pressure Sensor with Bluetooth capabilities containing a range of 0-400 Kilopascals (kPa) along with a capture collection rate maximum of 1000 Hertz (Hz)

2.6 Mass Balance

The mass balance used to record piping events has been used in previous piping studies. Studies conducted by Liang, Zeng, and Wan in 2017 use the mass balance to quantify the magnitude of piping as well as the time piping occurred (Liang et al., 2017). Using mass as a metric for observing piping can be useful, but using other methods such as pressure and turbidity along with mass can provide a greater understanding of how piping is initiated and allow for new advancements to be made.

Figure 11. Mass Balance capable of continuous data output at a rate of 1 Hertz that is displayed via graphing accumulated mass of sediment lost due to piping failure.

The mass balance is used to monitor live data and record the sediment expelled during the piping experiment, which is a BSK1100 model balance manufactured by PCE Instruments. This balance can record and display graphs of the mass live during experiments. The resolution of the balance is to 0.01g. In order to consistently record only the mass of sediment, a reservoir was placed on the scale that had overflow protection in place. This allowed for a constant mass of water to be present on the scale, thus only allowing the mass of sediment added to the reservoir to be recorded. To further assist with the consistency of measurement, a diffuser was put in place where the sediment enters

the reservoir. This diffuser allows for less turbulent release of sediment into the reservoir, thus limiting the unwanted spikes in mass further. This also allows for smaller sediments to not flow out the overflow protection and allows for all sediments to be captured. The balance with reservoir and overflow protection in place can be seen in image 11.

2.7 Turbidity Sensor

Even with the diffuser and mass balance in place, the fine particles in the silt classification remain suspended in the water, hence are unable to be properly recorded via mass. To capture these sediments, a turbidity sensor was placed on the outflow of the overflow protection from the mass balance. This allows for the fine silts to be captured and recorded, creating another metric to relate to piping events. The turbidity sensor used is an Apure TS-620 turbidity monitoring system. This system has a resolution of 0.01 Nephelometric Turbidity Units (NTU) and can measure values ranging from 0-400 NTU. This data is sent to the recorder and stored for download after completion of the experiment. Using this system allows for validity of the time piping occurred as the spike in NTU values can be easily distinguished via graphs. The magnitude of piping events can also be studied as a correlation can be made from amount of sediment captured on the mass balance to the value of NTU recorded from the turbidity meter.

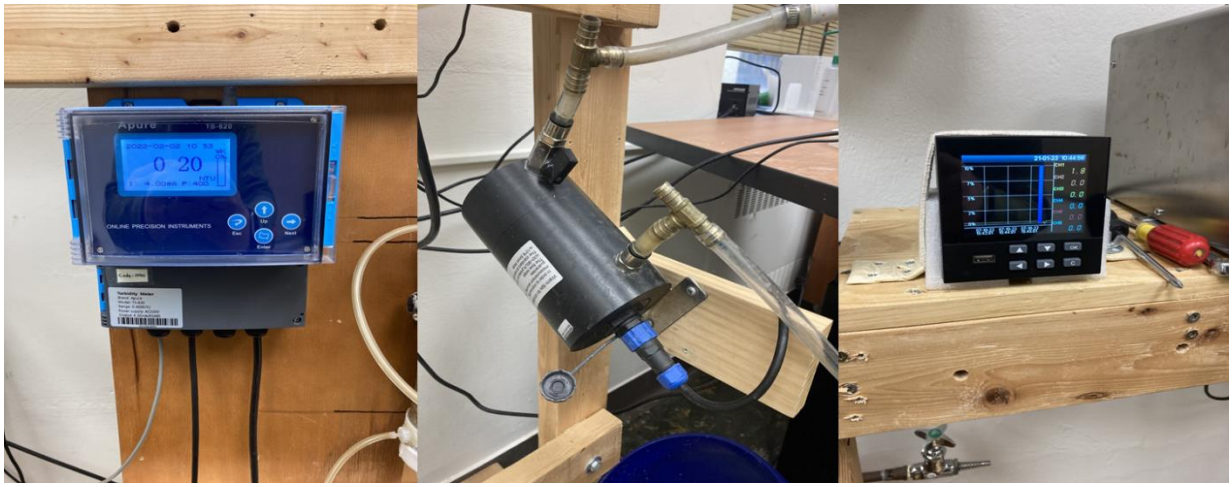

Figure 12. Turbidity Meter, Sensor, and Recorder. The turbidity meter displays the real time NTU value and is used for calibration of the sensor. The turbidity sensor records NTU values of the affluent water at a frequency of 1 Hertz, and the turbidity recorder collects the turbidity data for download via insertion of a USB drive.

Prior to use, the turbidity sensor must be calibrated. To achieve this, a two-point calibration is used. The sensor is removed from the cell and placed in two different solutions with known NTU values. These two solutions are deionized water (0 NTU) and a lab graded solution measuring at 280 NTU. The sensor is then placed into the solution in a completely dark room, removing any chance for interference with readings. While submerged in the solutions, the value of the solution is then input into the recorder, calibrating to that solution. An image of the turbidity meter, sensor, and recorder are shown in image 12.

2.8 Flow Rate Strategy to Test Piping at Desired Hydraulic Gradient

To accurately conduct and collect data from the piping tests and provide a stable means for repeatability, a consistent method must be used to saturate the sample and increase the gradient applied to the sample. Saturation is achieved by introducing fluid flow at a velocity low enough that the hydraulic gradient is less than one. As stated previously, piping occurs at a gradient of one (Atallah, 2013). This gradient applied slowly saturates the sample and is run for three hours to ensure no air is present in the sample.

Once saturation is achieved, the gradient is gradually increased until a gradient of one is attained. The velocity recorded to reach the gradient of one is kept constant, and any change in gradient is recorded via the change in pressure within the column. After this initial gradient is reached, the velocity is held constant for one hour with no change recorded. If there is change in gradient recorded, the velocity is held constant until changes in gradient cease a stable gradient is achieved. Once either one of these criteria is met, the velocity is steadily increased, also increasing the hydraulic gradient until a factor of one magnitude is gained. This increase in gradient is done slowly over a five-minute interval in order to mitigate the manual onset of piping. The same criteria are implemented as when to increase gradient for subsequent gradients until piping failure occurs.

3.0 Results

3.1 Data Analysis Methodology

The methodology for analyzing and comparing data obtained via the pressure sensors, mass balance, and turbidity sensor is unique to this experimentation as each component can be used as a metric to determine the onset of piping along with the magnitude. The use of the pressure sensor allows for observation of piping events that are unable to be captured via the mass balance and turbidity sensor. Clogging and de-clogging events are able to be captured when no sediment is lost within the column. These events structurally affect the column without any sediment being lost and can greatly affect the threshold of the onset of piping phenomena. The opportunity to capture these internal events would be lost if only the mass balance and turbidity sensor were used as metrics of identifying the onset of piping. The turbidity sensor plays a similar role as fines lost within the sample would evade being recorded via the mass balance due to remaining in suspension within the affluent water. Allowing for these fines to be observed is

critical to the research as the loss of these fines creates larger pore spaces within the soil media, allowing for piping to occur more readily.

It is important to note that as the experiment is being conducted and a manual increase is shown, an increase in mass can also be seen. This is not due to mass being expelled but rather the increase in flow of affluent water being released onto the mass balance. This can be confirmed as the mass data remains constant after the increase of the gradient. Mass data can be seen when there is an increase in mass when no manual increase was performed.

The resulting piping data compiled from the conducted studies is displayed in terms of the coefficient of uniformity. Along with this, other correlations are made and displayed in ways that can depict trends throughout the data.

3.2 Time evolution piping of Cu 1.5

The evolution of piping within the confines of a Cu of 1.5 is displayed in figure 13. Depicted within the figure are clear indications of manual increase of gradient as well as naturally occurring clogging and piping events. Along with pressure and mass data of each experiment pertaining to the constraints of the Cu of 1.5, the turbidity and conductivity is included and overlain. Regarding figure 13, the three experiments conducted behaved similarly in terms of time. Of the three Cu values tested, the values of 1.5 experienced failure in the shortest timeframe ranging from two to five hours. The gradient at which piping onset also was similar and ranged from three to five. The turbidity was only captured at the d50 of 300 microns, smallest d50 studied. In the remaining two d50 values no fines were captured as lost in the sample. The conductivity values directly reflect the pressure data. When the final gradient is reached, an increase in conductivity is recorded. Figure 13, subfigure *a* depicts mass extruded

and hydraulic gradient for a soil with a d_{50} of 1.093mm and a C_u of 1.5. Figure 13, subfigure *b*

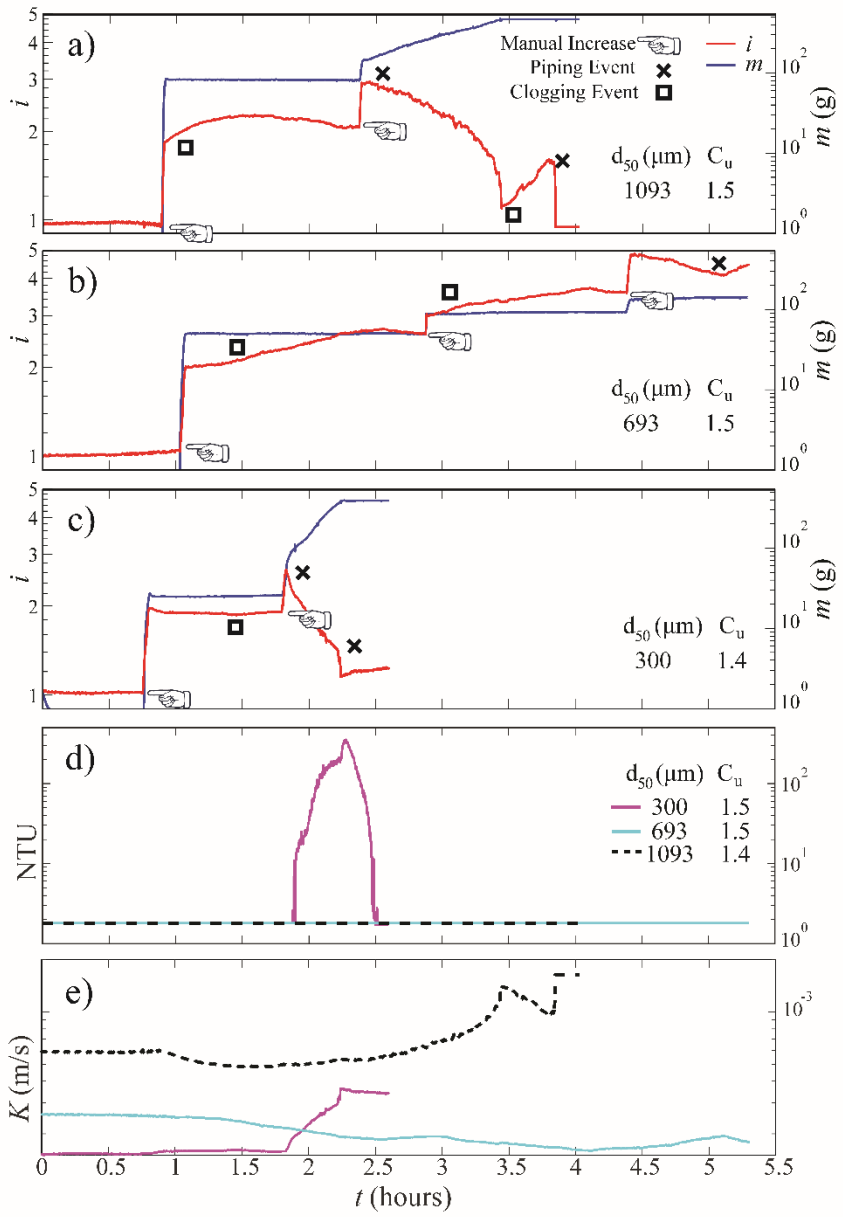

Figure 13. a) Time evolution of piping within a sediment containing a C_u of 1.5 and a d_{50} of 1093μm. b) Time evolution of piping within a sediment containing a C_u of 1.5 and a d_{50} of 693μm. c) Time evolution of piping within a sediment containing a C_u of 1.4 and a d_{50} of 300μm. d) Time evolution of turbidity (NTU) for sediments with an average C_u of 1.5. e) Time evolution of hydraulic conductivity (K) for sediments with an average C_u of 1.5.

depicts mass extruded and hydraulic gradient for a soil with a d_{50} of 0.693mm and a C_u of 1.5. Figure 13, subfigure *c* depicts mass extruded and hydraulic gradient for a soil with a d_{50} of 0.300mm and a C_u of 1.4. Figure 13, subfigure *d* depicts the recorded turbidity values for the three soil samples observed in figure 13, subfigure *a*, *b*, and *c*. Figure 13, subfigure *e* depicts the hydraulic conductivity values for the three soil samples observed in figure 13, subfigure *a*, *b*, and *c*.

3.3 Time evolution piping of Cu 3.3

The evolution of piping within the confines of an average Cu of 3.3 is displayed in figure 14. Figure 14, subfigure *a* depicts mass extruded and hydraulic gradient for a soil with a d_{50} of 0.994mm and a C_u of 2.8. Figure 14, subfigure *b* depicts mass extruded and hydraulic gradient for a soil with a d_{50} of 0.736mm and a C_u of 3.1. Figure 14, subfigure *c* depicts mass extruded and hydraulic gradient for a soil with a d_{50} of 0.350mm and a C_u of 3.3. Figure 14, subfigure *d* depicts the recorded turbidity values for the three soil samples observed in figure 14, subfigure *a*, *b*, and *c*. Figure 14, subfigure *e* depicts the hydraulic conductivity values for the three soil samples observed in figure 14, subfigure *a*, *b*, and *c*. A clear change from this set of experiments to the previous is the number of manually increased gradients taken to reach failure. The length of time taken to reach piping failure has also increased to eight to 10 hours. These changes allow for phenomena such as clogging events to be better studied within the experiment. Subgraph *a* within figure 14 depicts a prime example of clogging-piping events while no visible sediments are extruded from the sample from a timeframe of 3 to 6 hours. This phenomenon is observed throughout most experiments and vital to the study of piping. These events of clogging and piping with no large failure occurring were allowed to occur until a stable gradient is achieved. These minor clogging and piping events can be attributed to the rearranging of sediments within

the column. Without the pressure sensor, these small events may go unnoticed. Increasing the gradient manually while these fluctuations in gradient are occurring could allow for early onset

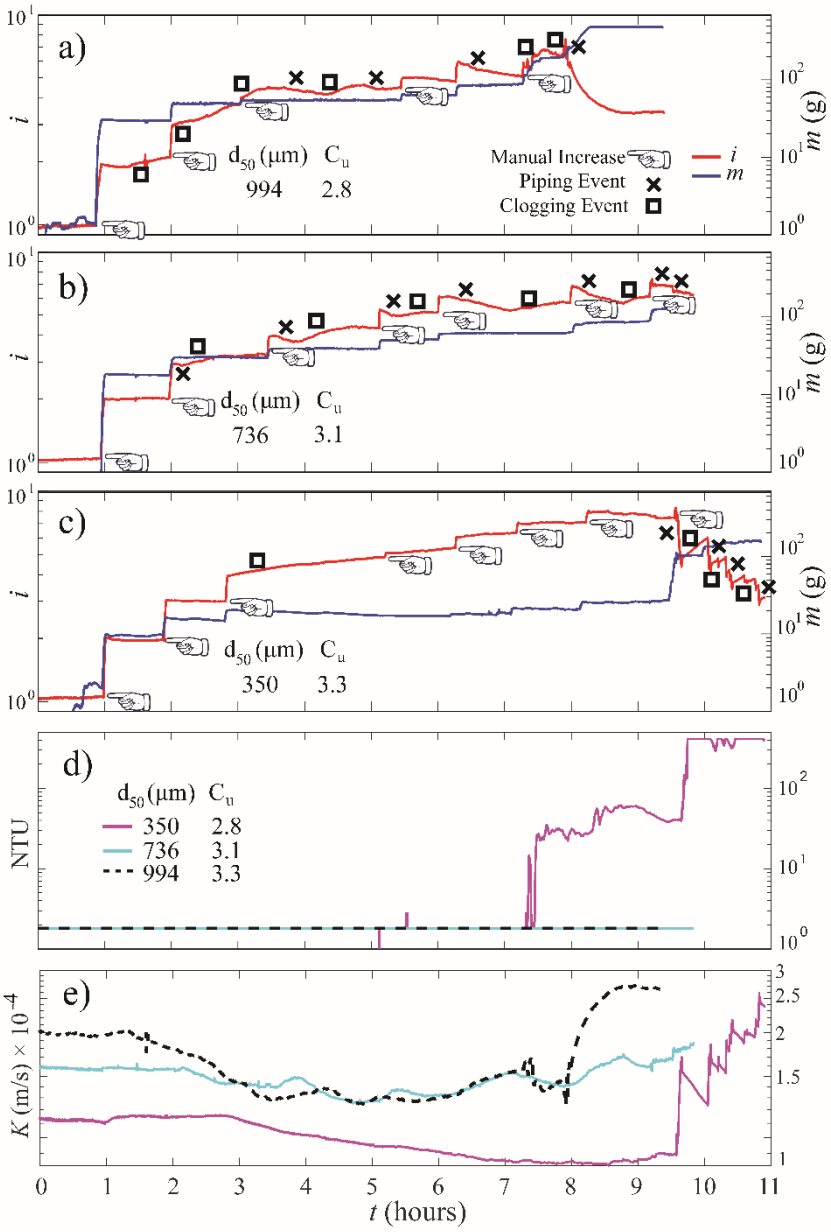

Figure 14. a) Time evolution of piping within a sediment containing a Cu of 2.8 and a d_{50} of 994μm. b) Time evolution of piping within a sediment containing a C_u of 3.3 and a d_{50} of 736μm. c) Time evolution of piping within a sediment containing a C_u of 3.3 and a d_{50} of 350μm. d) Time evolution of turbidity (NTU) for sediments with an average C_u of 3.3. e) Time evolution of hydraulic conductivity (K) for sediments with an average C_u of 3.3.

of piping as the sediment particles have not fully been allotted the time to reach their state of equilibrium. As with the graphs depicting the piping experiments with a Cu of 1.5, these experiments only recorded turbidity within the mixture having the smallest d50 at 350 microns.

3.4 Time evolution piping of Cu 6.5

The evolution of piping within the confines of a Cu of 6.5 is displayed in figure 15. Figure 15, subfigure *a* depicts mass extruded and hydraulic gradient for a soil with a d_{50} of 0.990mm and a C_u of 6.25. Figure 15, subfigure *b* depicts mass extruded and hydraulic gradient for a soil with a d_{50} of 0.784mm and a C_u of 6.75. Figure 15, subfigure *c* depicts mass extruded and hydraulic gradient for a soil with a d_{50} of 0.350mm and a C_u of 6.75. Figure 15, subfigure *d* depicts the recorded turbidity values for the three soil samples observed in figure 15, subfigure *a*, *b*, and *c*. Figure 15, subfigure *e* depicts the hydraulic conductivity values for the three soil samples observed in figure 13, subfigure *a*, *b*, and *c*. Again, it is noticeable that there has been a larger number of manual increases taken to reach piping failure than the previous two sets of experiments with smaller Cu values. The time to piping failure has also increased to a timeframe of 12 to 14 hours. The distinct difference in this data set can be noticed with observing the turbidity, as all three d50 distributions expelled fines within the duration of the experiment. It is crucial to observe the loss of these fines via the turbidity meter as there is no increase in mass that correlates to the increase in turbidity. As previously mentioned, this is due to the fines remaining in suspension of the affluent water, thus not able to be captured via mass balance readings.

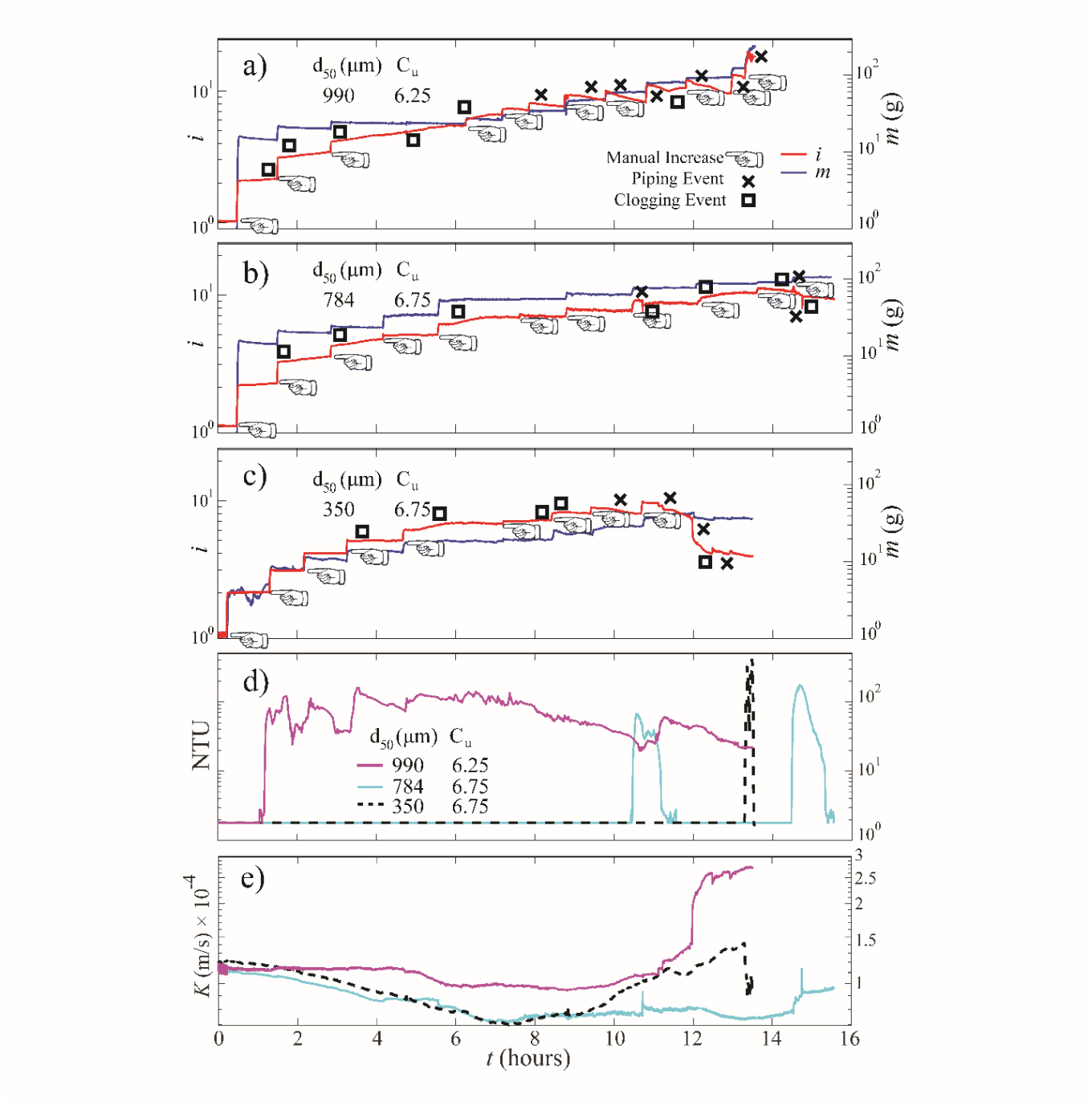

Figure 15. a) Time evolution of piping within a sediment containing a Cu of 6.25 and a d_{50} of 990μm. b) Time evolution of piping within a sediment containing a C_u of 6.75 and a d_{50} of 784μm. c) Time evolution of piping within a sediment containing a C_u of 6.75 and a d_{50} of 350μm. d) Time evolution of turbidity (NTU) for sediments with an average C_u of 6.5. e) Time evolution of hydraulic conductivity (K) for sediments with an average C_u of 6.5.

3.5 Gradient at Final Failure (i_f) vs Sediment Characteristics

The i_f is defined as the gradient at which the final piping failure occurred. Plotting the i_f against the d_{50} and the C_u of each sediment mixture created can allow for some correlations to be seen.

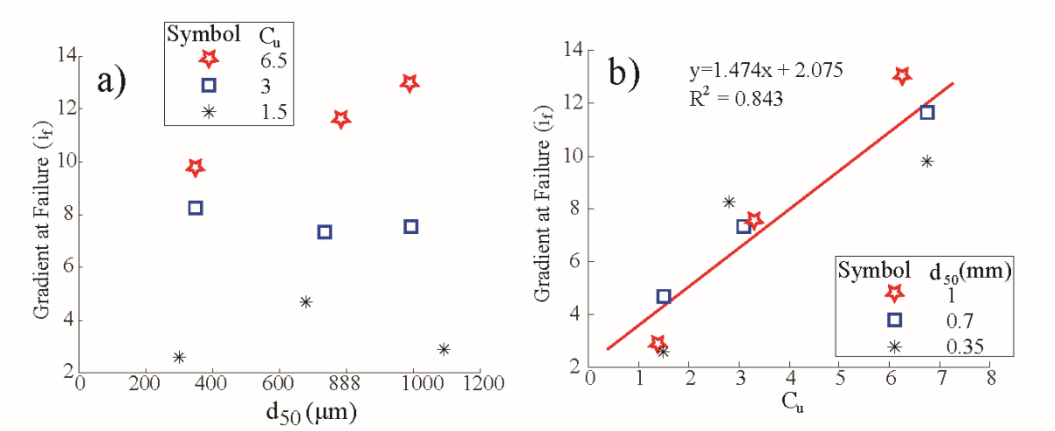

Figure 16.a) Gradient at failure vs. d_{50}. The gradient at failure is the hydraulic gradient recorded when the given sediment reaches the final piping failure. b) Gradient at failure vs. C_u.

As seen in figure 16, subfigure *a*, the smaller the d_{50} of a sediment, the lower the gradient at which final failure will occur can be expected to be. When comparing the d_{50} of a sediment sample to the C_u value, a correlation can be seen that allows for a trendline to be applied to the data. As seen with the d_{50} dataset, the lower the C_u in a sediment mixture, the lower the gradient at which piping will occur as displayed in subfigure *b*. The trendline of this dataset returns an R^2 value of 0.843.

3.6 Gradient at Final Failure (i_f) vs Applied Gradient

Figure 17 exhibits a relationship between the applied gradient and the gradient at final failure. Applied gradient is calculated via dividing conductivity (K) by flow rate (Q) that led to the final failure event, i.e., Q/KA, where A is the area of cross-section. Upon imposing the flow rate that led to the final failure event, gradient evolves until the final state, leading to the final failure event which is recorded by the pressure sensor. We compare these two gradient states to identify how heterogeneity of a soil contribute to the piping failure threshold.

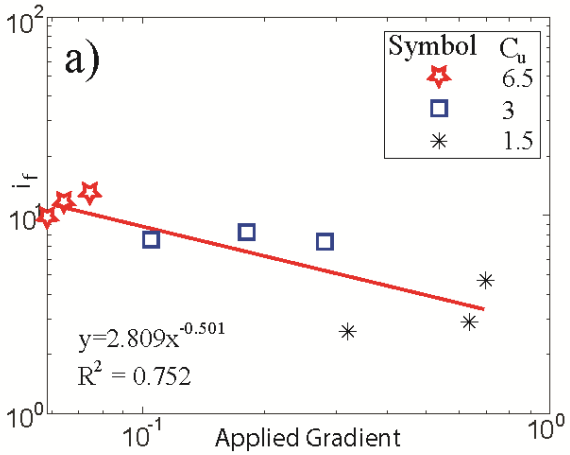

Figure 17. a) Gradient at Failure vs Applied Gradient. The gradient at failure is the hydraulic gradient recorded when the given sediment reaches the final piping failure and the applied gradient is calculated by dividing the conductivity (K) by the flow rate (Q) that lead to the final piping failure.

With a trendline exhibiting an R-squared value of 0.752, using this relationship can allow predictions to be made on when a certain soil will become susceptible to piping.

3.7 Volumetric Flux (Q_{pump}) at final failure vs Sediment Characteristics

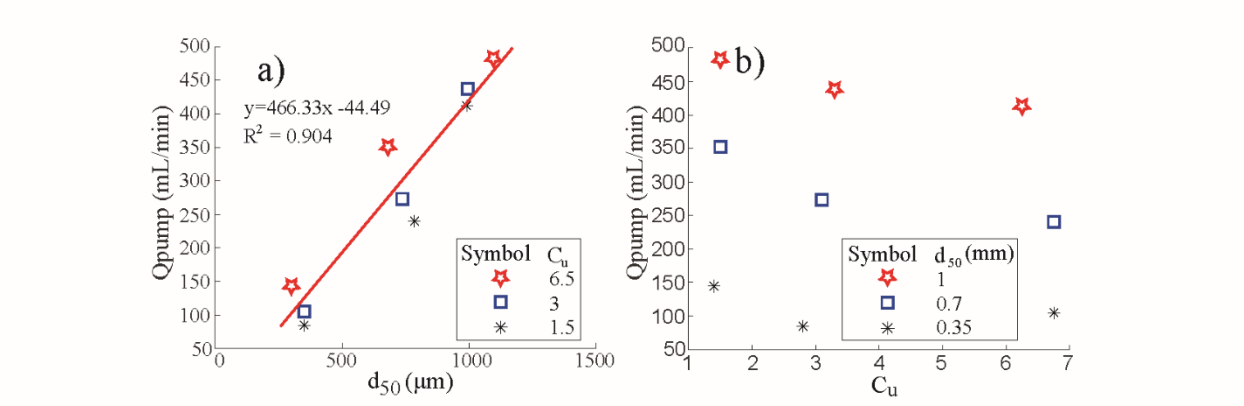

Figure 18. a) Volumetric Flux (Q_{pump}) at Final Failure vs d_{50}. Volumetric flux is the is the rate at which the pump was running during the final piping failure event. b) Volumetric Flux (Q_{pump}) at Final Failure vs C_u

Figure 18 depicts the volumetric flux of the pump during failure (Q_{pump}) vs the d_{50} and C_u values of each sediment mixture. A trendline with an R^2 value of 0.904 is able to be applied to the graph depicting Q_{pump} vs the d_{50} values as seen in subfigure *a*. Based on the graphs, the larger the d_{50} value, the larger the Q_{pump} must be to achieve final failure. Along with this same ideology, the larger the C_u, the larger the Q_{pump} must be to achieve final failure as shown in subfigure *b*.

3.8 Time to Final Failure vs Cu and Porosity

The time it takes for a sediment to reach final piping failure can be related to the C_u and porosity of that given sediment. As seen in figure 19, trendlines can be fit within the data to depict a relationship that gives a metric for piping occurrence. Based on the graphs, the higher the C_u value is within a sediment mixture, the longer it will take for piping to take place as depicted in subfigure *a*. In a similar manner, the lower the porosity within the sediment matrix, the longer it will take for piping to occur as depicted in subfigure *b*. Porosity was calculated via

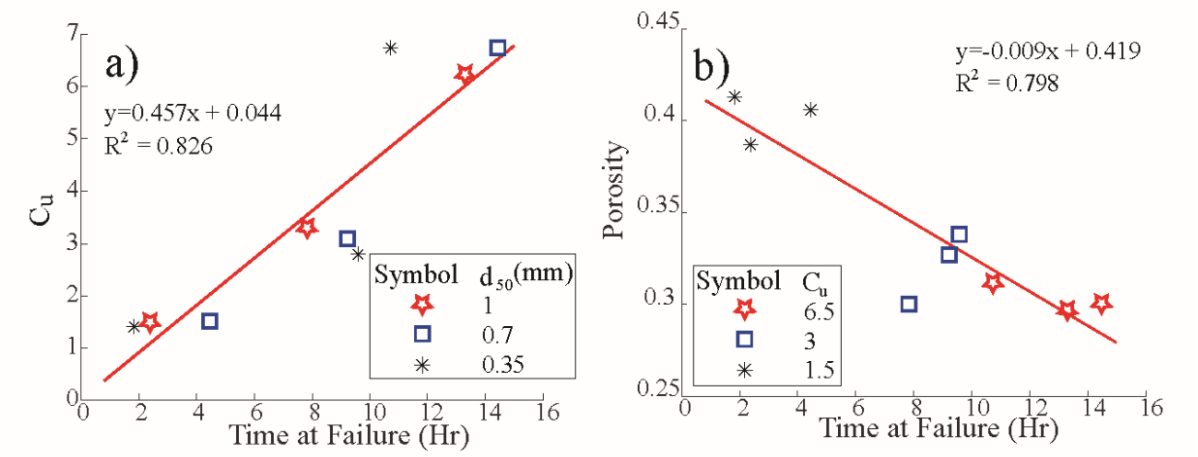

Figure 19. a) Time to Failure vs C_u. Time to failure is the time taken to reach the final piping failure event. b) Time to Failure vs Porosity. Porosity is calculated via $\varphi = 1 - \rho_b/\rho_p$.

following $\varphi = 1 - \rho_b/\rho_p$, where φ is the porosity, ρ_b is the bulk density, and ρ_p is the particle density assumed to be 2.65 g/cm^3. To calculate bulk density of a sample. The sample was dried in an oven to remove all moisture for a duration of 8 hours. After drying, the mass of the dry

sample was divided by the volume to achieve the bulk density. The volume of the sample includes the soil particles as well as the pore spaces within the sample.

3.9 Failure rate vs. Sediment Characteristics

As seen in figure 20, relations can be made with the failure rate (f_r) of a sediment and the corresponding d_{50} and C_u values. The failure rate is determined by taking the slope of the hydraulic gradient during the final piping failure event. These slopes can be referenced in Appendix B. By analyzing the graphed data, the smaller the d_{50} of a given sediment mixture, the fail rate at smaller values of C_u don't appear to have any correlation depicted in subfigure *a*. However, as the C_u increases, a relationship becomes visible being that the smaller the d_{50}, the smaller the failure rate is as depicted in subfigure *b*.

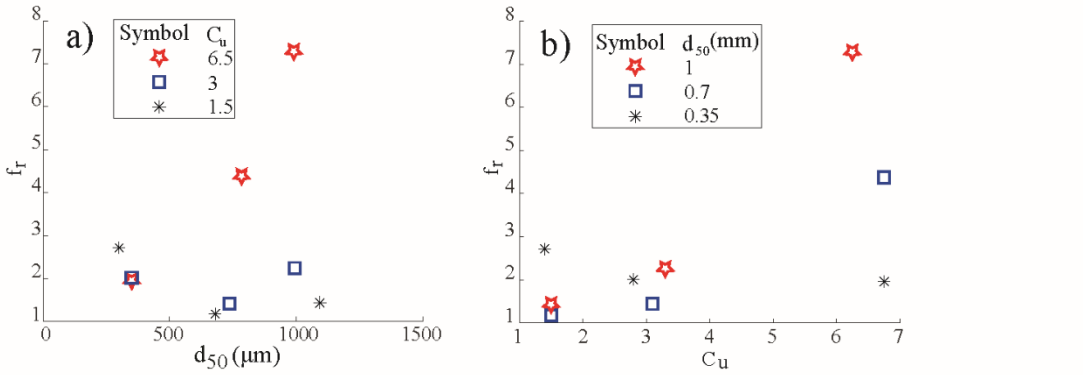

Figure 20. a) Failure Rate vs. d_{50}. The failure rate is determined by taking the slope of the hydraulic gradient during the final piping failure event b) Failure Rate vs C_u

3.10 Frequency of clogging and piping events

The frequency of clogging or piping event is simply the number of times a clogging or piping event occurred during experimentation of a given sample. A correlation is visible between the C_u of a sample and these events. Regarding C_u, the smaller the value, the less clogging events

take place. The same can be said for the piping events of a sample where the smaller the value of Cu the less piping events occur. Figure 22 depicts this data.

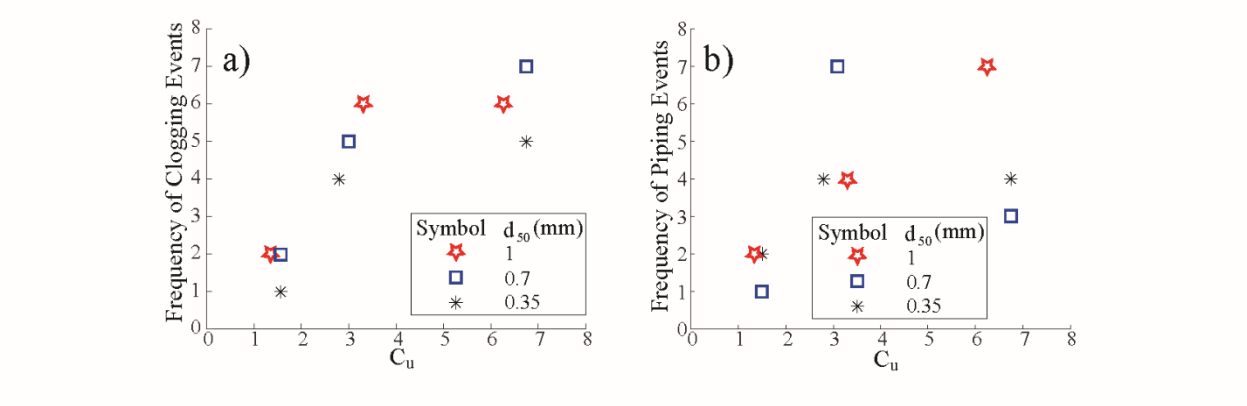

Figure 21. a) Frequency of Clogging Events vs. C_u. The frequency of clogging events is defined as the number of minute clogging events that took place during experimentation of a given soil. b) Frequency of Piping Events vs. C_u. The frequency of piping events is defined as the number of minute piping events that took place during experimentation of a given soil

4.0 Discussion

The data collected can be interpreted to provide correlations between experimental tests of differing soil heterogeneity and sediment size. Looking at the time taken to reach piping failure, a pattern can be observed that as the C_u of a soil is increased, the time taken for piping to occur also increases. This evidence is clearly depicted in figures 13, 14, and 15. Along with this, it is noted that as the C_u increases, the gradient needed for final failure to occur also increases. These findings confirm the hypotheses created prior to experimentation to be validated and correct.

4.1 Clogging and Unclogging Events

A new insight was also brought to light with this research. As the hydraulic gradient was manually and slowly increased, clogging and unclogging events were noticed via pressure sensor readings. This is caused by the rearranging of sediments within the column due to the increase in hydraulic pressure. This pressure is not strong enough to remove any sediment from the sample,

but regardless affects the structure and strength of the sample. These clogging and unclogging events are not able to be captured via mass balance as no mass is lost. Within samples of higher C_u values, the initial onset of these clogging events can be captured via loss of fines recorded by the turbidity meter. However, after these fines are lost, the clogging and unclogging events that continue to occur are only recordable via the pressure sensors. It is also noticed these clogging and unclogging events will stabilize, given the hydraulic gradient remains constant. The high sensitivity of the sensors used to capture this data allowed for this phenomenon to be clearly captured. This can be seen in figure 14, graph *a*. As the sample is induced to a hydraulic gradient of four, the pressure fluctuates while mass and turbidity remain constant. After two and a half hours, the pressure stabilizes and as no piping failure occurs, the gradient is manually increased. It is believed that these clogging and unclogging events can play a critical role in the piping failure of a soil. If a soil exhibits these characteristics and the sample isn't given time to stabilize, piping may occur at a lower gradient than expected.

4.2 Turbidity Correlations

Turbidity was a valuable metric collected to qualitatively define the magnitude and onsite of piping within soils containing fines. The larger the C_u value of the soil, the more data was collected in terms of turbidity as there are more fines present within the sample. As mentioned previously, these fines can indicate internal clogging and unclogging events. Turbidity can also be used to define the magnitude of piping failure, as the larger the NTU values recorded when failure occurred, the greater the mass lost from the sample is.

4.3 Conductivity Relations

Regarding conductivity, each experimental test exhibited a large change in conductivity during piping failure. Conductivity is determined by $k = i \,/\, (Q/A)$, where k refers to hydraulic

conductivity, *i* refers to hydraulic gradient, *Q* refers to the flow rate of the pump, and *A* refers to the cross-sectional area of the sample. Almost every experimental run depicted this as a large increase. This follows the theory of piping that conductivity increases with piping failure (Ke & Takahashi, 2014). Conductivity can also be used to depict the clogging and unclogging events discussed earlier. As clogging takes place, the conductivity decreases. As the unclogging takes place, conductivity increases. Conductivity provides a direct correlation to hydraulic gradient to allow for more understanding of piping phenomena in terms of hydraulic seepage flow.

4.4 Relations to Previous Work

The research conducted provided relations to previously conducted research on the piping phenomena topic that proves valuable by confirming findings in such previous work as well as affirming the research conducted is of high quality and is robust. Fleshman's research published in 2014 came to the similar conclusion that piping occurs at a higher hydraulic gradient as the soil becomes more graded. Fleshman also makes note of a change in conductivity early in experimentation before piping failure occurs. It is briefly explained this is due to loosening of surface material as flow is induced. This process can be recognized as the onset of clogging and unclogging events that are prevalent within this research conducted. No further analysis is done on this important phenomenon within Fleshman's publication (Fleshman & Rice, 2014).

Ke and Takashi in their 2014 publication made the statement that after piping failure occurs, there is a large change in hydraulic conductivity (Ke & Takahashi, 2014). This was able to be confirmed via the use of pressure sensors. Relating pressure to conductivity is done via the equation mentioned in section 4.3 of this paper. Graph *d* within figures 13, 14, and 15 depict the conductivity values, and the change in conductivity is evident and can be associated to piping failure.

Atallah (2013), states that piping failure can occur at hydraulic gradients as low as one (Atallah et al., 2013). This is accepted to be true, but during experimentation of this research, that was never achieved. Due to this widely accepted statement, all samples were saturated at a gradient of less than one. When the gradient was increased to one, the hydraulic gradient remained constant. This is most likely linked to the selection of samples tested. The smallest homogeneous sample created is that of a d_{50} value of 0.3mm, which is defined as a medium sand (refer to table 1). In order to achieve piping at a gradient of one, fine to very fine sands may need to be utilized as the lowest homogenous sample.

4.5 Further Research Needs

This research provides high quality data that gives a robust starting point for future research following the same experimental procedure. It has been studied in depth previously that piping can occur more readily along sediment size boundaries commonly found in gap-graded soils (Ke & Takahashi, 2014; Nguyen et al., 2013; Zhang et al., 2020). Conducting experimentation on such soils could provide a unique outlook on another scenario where piping occurs.

Taking boundary conditions into account would be a valuable study for this research. Piping conditions were noted to take place internally as during experimentation no piping behavior was noted visually, however piping events were recorded on the sensors in use. Regardless it is important to test the idea that piping may tend to occur along the boundary of the soil/plexiglass interface. Repeating this experimentation with a cylinder of larger diameter would prove valuable to depict how piping phenomena behaves under a larger cross-sectional area.

Another aspect that could be touched upon is the introduction of clay material to the mixtures. Clay would remove the cohesionless properties of the mixtures, thus it is expected that

a higher hydraulic gradient must be present in order to induce piping failure. Chemical properties would also need to be taken into consideration, adding complexity to experimentation. A study conducted by Grabowski et al. (2011) was done to examine the piping threshold of soils based on the SAR levels. Two soils were examined in the study, one consisting of pure montmorillonite and the other consisting of mostly kaolinite. It was noted in the research that the soil containing pure montmorillonite had a higher shear strength than that of the kaolinite soil given the SAR in the water introduced to the soil was elevated. If the SAR in the water is reduced, the kaolinite soil will express the higher shear strength (Grabowski, et al 2011).

The relative density (actual density/maximum dry density) of a soil can influence its piping potential. As density of a soil increases, its piping potential decreases. As a soil becomes more dense, angular grains in a soil can interlock and become stable, preventing the removal of the grains via piping. A soil that is less dense does not convey the interlocking grains, thus creating a media that more readily pipes. Studying different densities of similar soils may provide more data on the initiation and threshold of piping that could prove valuable.

The analysis of the sediments lost due to piping events would be valuable in future research. Referencing sediment characteristics of the sediment lost due to piping of differing soil mixtures may provide correlations not discovered in this study. It would prove valuable to also create a grain size distribution curve and obtain sediment characteristics of the sample subject to piping after final failure occurs.

5.0 Conclusion

We show piping failure or piping potential is directly related to the grain size and heterogeneity of a soil mixture via the use of data collected with high sensitivity. A soil with a smaller d_{50} experiences piping failure at a lower hydraulic gradient than that that of a soil with a

larger d_{50}. A soil with a smaller C_u, i.e., well-sorted sediments, experience piping failure at a lower hydraulic gradient than that that of a soil with a larger C_u or well-graded soil. The use of pressure sensors monitoring hydraulic gradient in real time proved vital as clogging and unclogging events were able to be captured prior to piping failure. Monitoring these clogging and piping events allows for the correlation to be made that as the C_u of a soil increases, the number of these minor events increases (as seen in figure 22), but the time to failure also increases (as seen in figure 19).

These clogging and unclogging events provide a topic to be further studied in future research to better provide insight on how these events influence piping failure. The mass collection system provided further data on capturing piping events and depicting their magnitude. Further research on these sediments lost due to piping failure could prove valuable to the study of how samples are altered pre and post-piping.

Piping has been studied thoroughly in the field and in a laboratory setting. However, glaciation has altered a large portion of the northern United States. This glaciation leaves the land composed of many differing soil types as a result of glacial till. As no two soils behave the same, there would have to be many tests conducted to properly conclude the threshold of piping potential within a region. The chosen soils are known to readily pipe, so the altercation of the soil's grain size distribution could be the focal point of the study. With the conclusion of this research, it is hoped that future research can expand and further explore a soils ability to pipe in relation to the grain size distribution of the soil.

6.0 References

ALsakran, M. A., Zhu, J. G., & Er-lu, W. (2021). Experimental Study for Assessing the Onset of Suffusion and Suffosion of Gap-Graded Soil. *Soil Mechanics and Foundation Engineering*, *57*(6), 458–464. https://doi.org/10.1007/s11204-021-09693-4

American Society for Testing and Materials (ASTM), 2010, Annual Book of Standards: Section 4, Construction, 4.08, Soil and Rock (1), West Conshohocken, PA.

Atallah, N. W., Shakoor, A., & Holm, D. (2013). *AN INVESTIGATION OF THE ORIGIN OF ROCK CITY AND CAUSE OF PIPING PROBLEMS AT MOUNTAIN LAKE, GILES COUNTY, VIRGINIA*.

Bernatek-Jakiel, A., & Poesen, J. (2018). Subsurface erosion by soil piping: significance and research needs. In *Earth-Science Reviews* (Vol. 185, pp. 1107–1128). Elsevier B.V. https://doi.org/10.1016/j.earscirev.2018.08.006

Chang, D. S., & Zhang, L. M. (2013). Critical Hydraulic Gradients of Internal Erosion under Complex Stress States. *Journal of Geotechnical and Geoenvironmental Engineering*, *139*(9), 1454–1467. https://doi.org/10.1061/(asce)gt.1943-5606.0000871

Fleshman, M., & Rice, J. (2014). Laboratory Modeling of the Mechanisms of Piping Erosion Initiation. *American Society of Civil Engineers*.

Grabowski, R. C., Droppo, I. G., & Wharton, G. (2011). Erodibility of cohesive sediment: The importance of sediment properties. In *Earth-Science Reviews* (Vol. 105, Issues 3–4, pp. 101–120). https://doi.org/10.1016/j.earscirev.2011.01.008

Holtz R. D. Kovacs, W.D., *An Introduction to Geotechnical Engineering*. Englewood Cliffs New Jersey: Prentice-Hall; 1981.

Holtz, R. D. Kovacs, W. D., & Sheahan, T. C. (2011). *An Introduction to Geotechnical Engineering* (2nd edition). Pearson Education, Inc.

Indraratna, B., Nguyen, V. T., & Rujikiatkamjorn, C. (2011). Assessing the Potential of Internal Erosion and Suffusion of Granular Soils. *Journal of Geotechnical and Geoenvironmental Engineering*, *137*(5), 550–554. https://doi.org/10.1061/(asce)gt.1943-5606.0000447

Israr, J., Indraratna, B., & Asce, F. (2019). *Study of Critical Hydraulic Gradients for Seepage-Induced Failures in Granular Soils*. https://doi.org/10.1061/(ASCE)

Ke, L., & Takahashi, A. (2012). Strength reduction of cohesionless soil due to internal erosion induced by one-dimensional upward seepage flow. *Soils and Foundations*, *52*(4), 698–711. https://doi.org/10.1016/j.sandf.2012.07.010

Ke, L., & Takahashi, A. (2014). Experimental investigations on suffusion characteristics and its mechanical consequences on saturated cohesionless soil. *Soils and Foundations*, *54*(4), 713–730. https://doi.org/10.1016/j.sandf.2014.06.024

Liang, Y., Zeng, C., Wang, J. J., Liu, M. W., Jim Yeh, T. C., & Zha, Y. Y. (2017). Constant gradient erosion apparatus for appraisal of piping behavior in upward seepage flow. *Geotechnical Testing Journal*, *40*(4), 630–642. https://doi.org/10.1520/GTJ20150282

Luo, Y. long, Wu, Q., Zhan, M. li, Sheng, J. chang, & Wang, Y. (2013). Hydro-mechanical coupling experiments on suffusion in sandy gravel foundations containing a partially

penetrating cut-off wall. *Natural Hazards*, *67*(2), 659–674. https://doi.org/10.1007/s11069-013-0596-z

Nguyen, D. M., Plé, O., & Monnet, J. (2013). Experimental study of suffusion in granular soils. *Advanced Materials Research*, *684*, 101–105. https://doi.org/10.4028/www.scientific.net/AMR.684.101

Oueidat, M., Benamar, A., & Bennabi, A. (2021). Effect of Fine Particles and Soil Heterogeneity on the Initiation of Suffusion. *Geotechnical and Geological Engineering*, *39*(3), 2359–2371. https://doi.org/10.1007/s10706-020-01632-8

Richards, K. S., & Reddy, K. R. (2010). *True Triaxial Piping Test Apparatus for Evaluation of Piping Potential in Earth Structures*.

Skempton, A. W., & Brogan, J. M. (1994). *Experiments on piping in sandy gravels* (Vol. 44, Issue 3).

TERZAGHI, K. (1939). 45TH JAMES FORREST LECTURE, 1939. SOIL MECHANICS - A NEW CHAPTER IN ENGINEERING SCIENCE. *Journal of the Institution of Civil Engineers*, *12*(7), 106–142. https://doi.org/10.1680/ijoti.1939.14534

Tian, D., Xie, Q., Fu, X., & Zhang, J. (2020). *Experimental study on the effect of fine contents on internal erosion in natural soil deposits*. https://doi.org/10.1007/s10064-020-01829-4/Published

Wilson, G., Bernatek-Jakiel, A., Nieber, J. L., and Fox, G. A.: Internal Erosion of Soil Pipes: Still More Questions Than Answers, EGU General Assembly 2020, Online, 4–8 May 2020, EGU2020-1497, https://doi.org/10.5194/egusphere-egu2020-1497, 2019

Wilson, G. V, Nieber, J. L., Sidle, R. C., & Fox, G. A. (2013). INTERNAL EROSION DURING SOIL PIPEFLOW: STATE OF THE SCIENCE FOR EXPERIMENTAL AND NUMERICAL ANALYSIS. *Transactions of the ASABE*, *56*(2), 465–478.

Zhang, F., Zhang, L., & Li, Y. (2020). Investigation of gap-graded soils' seepage internal stability with the concept of void filling ratio. *PLoS ONE*, *15*(2 February). https://doi.org/10.1371/JOURNAL.PONE.0229559

Appendix A

Below are the grain size distributions for the differing bins of sediment used in the research.

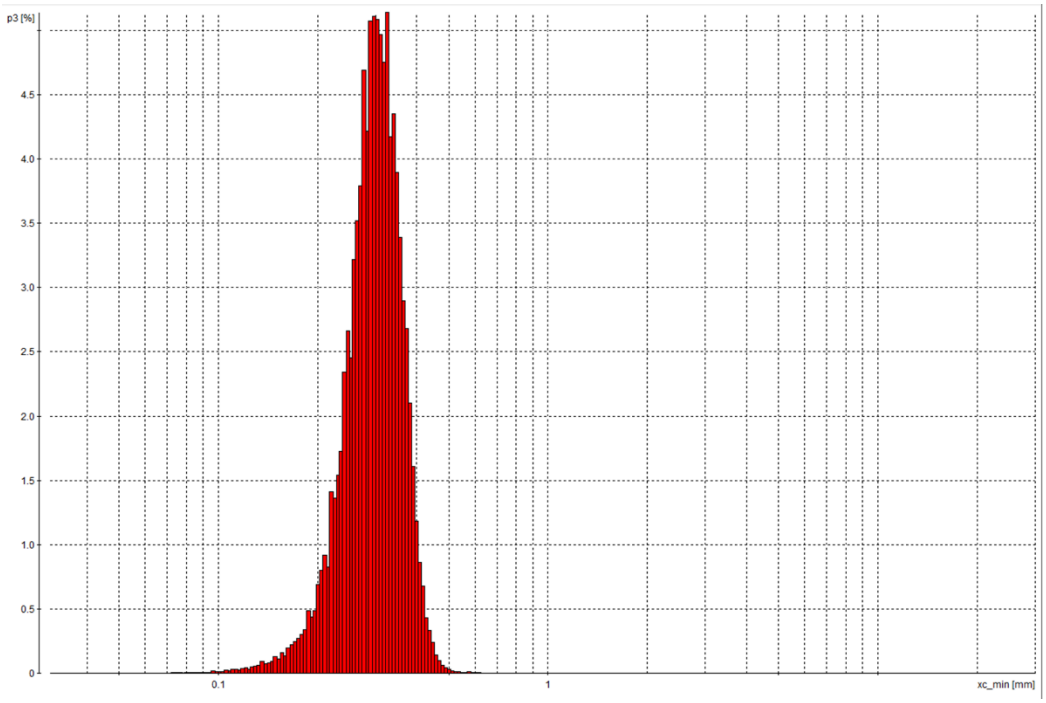

Figure 22. d50 of 0.300mm / Cu of 1.4 Camsizer Distribution

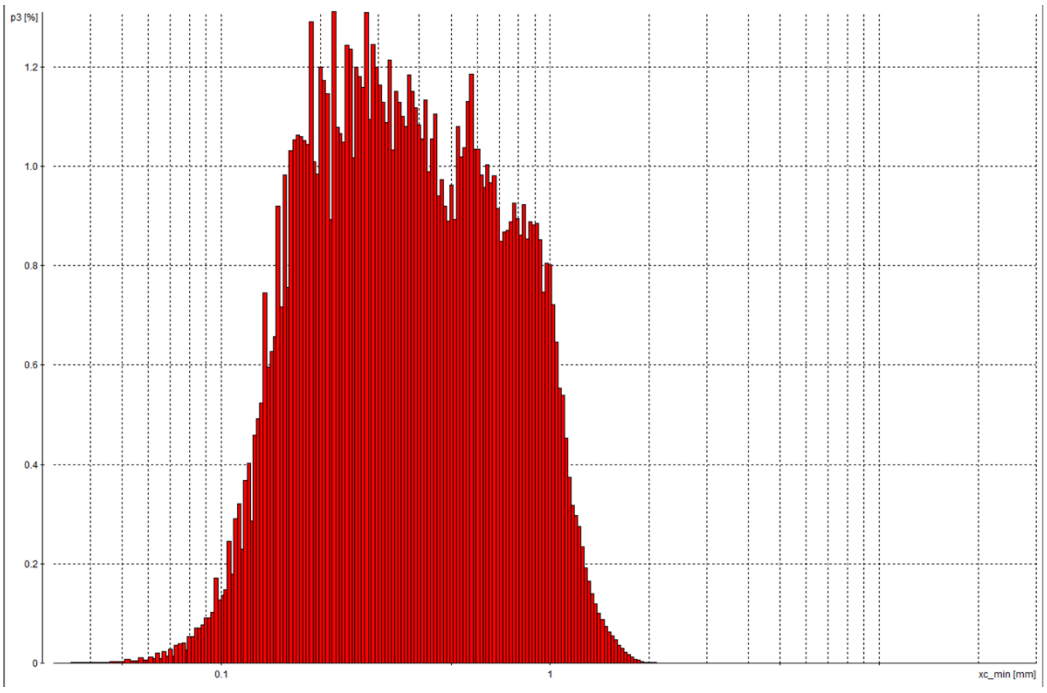

Figure 23. d50 of 0.350mm / Cu of 2.8 Camsizer Distribution

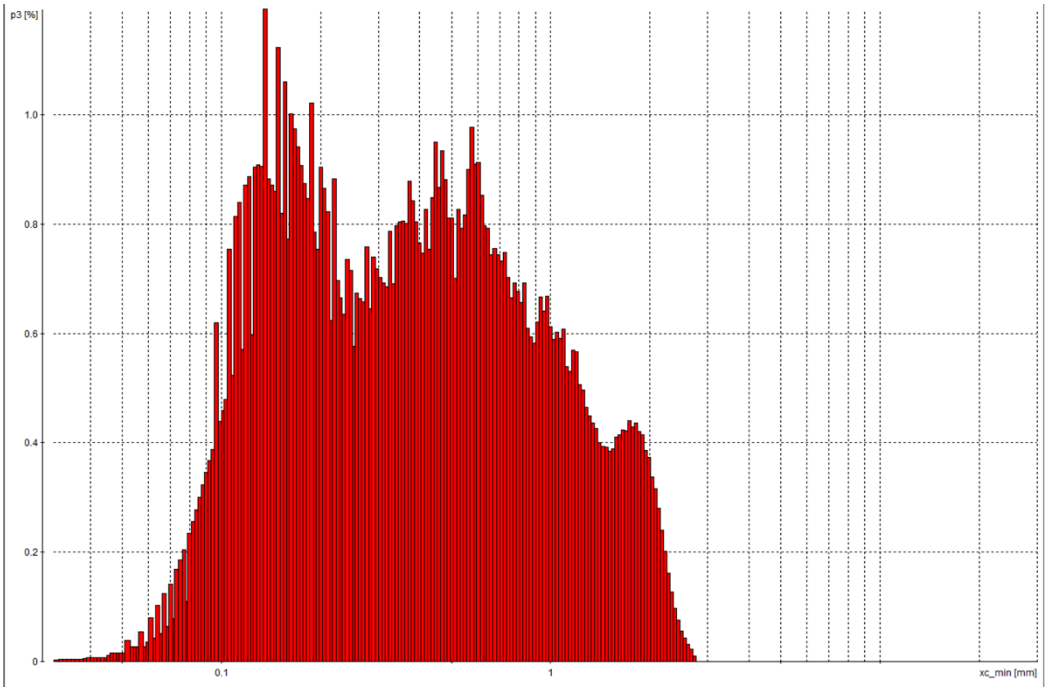

Figure 24. d50 of 0.350mm / Cu of 6.75 Camsizer Distribution

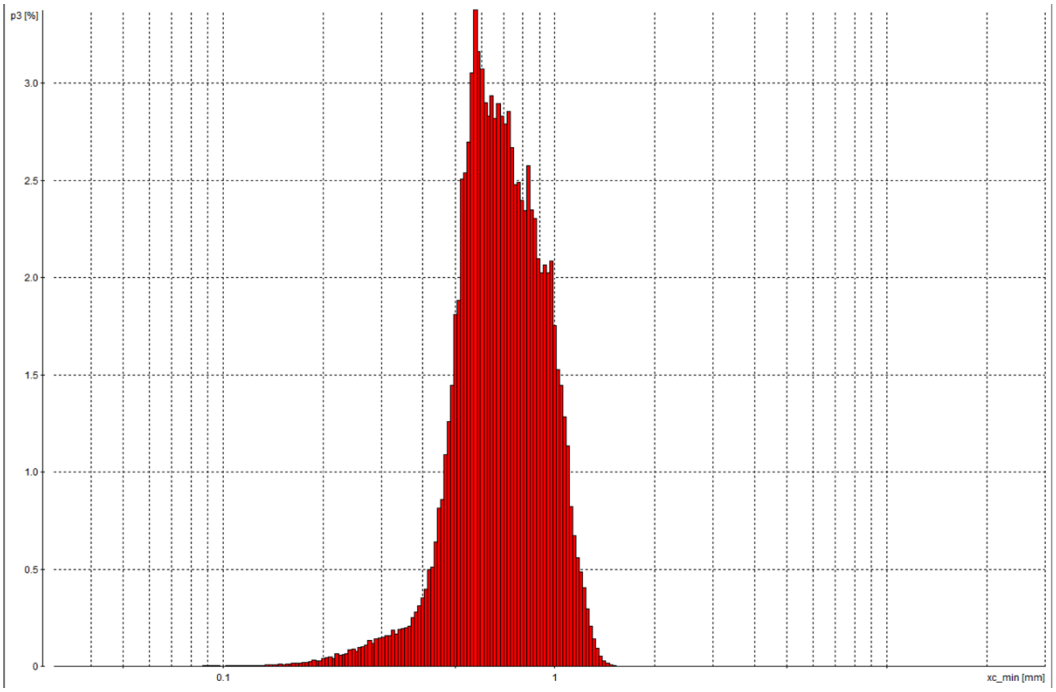

Figure 25. d50 of 0.693mm / Cu of 1.5 Camsizer Distribution

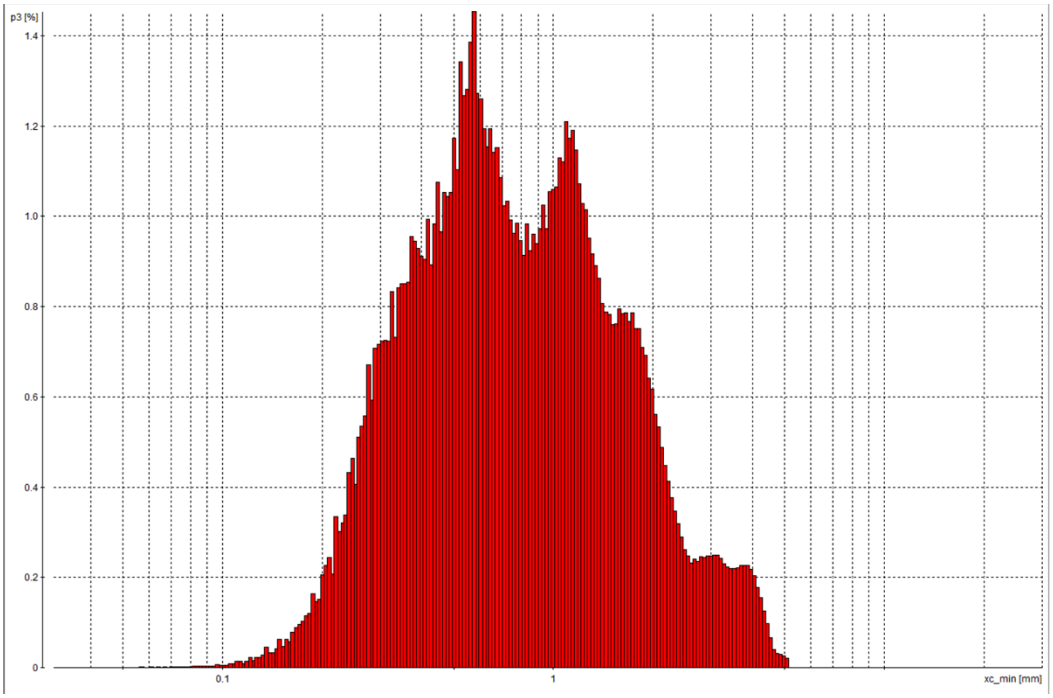

Figure 26. d50 of 0.736mm / Cu of 3.1 Camsizer Distribution

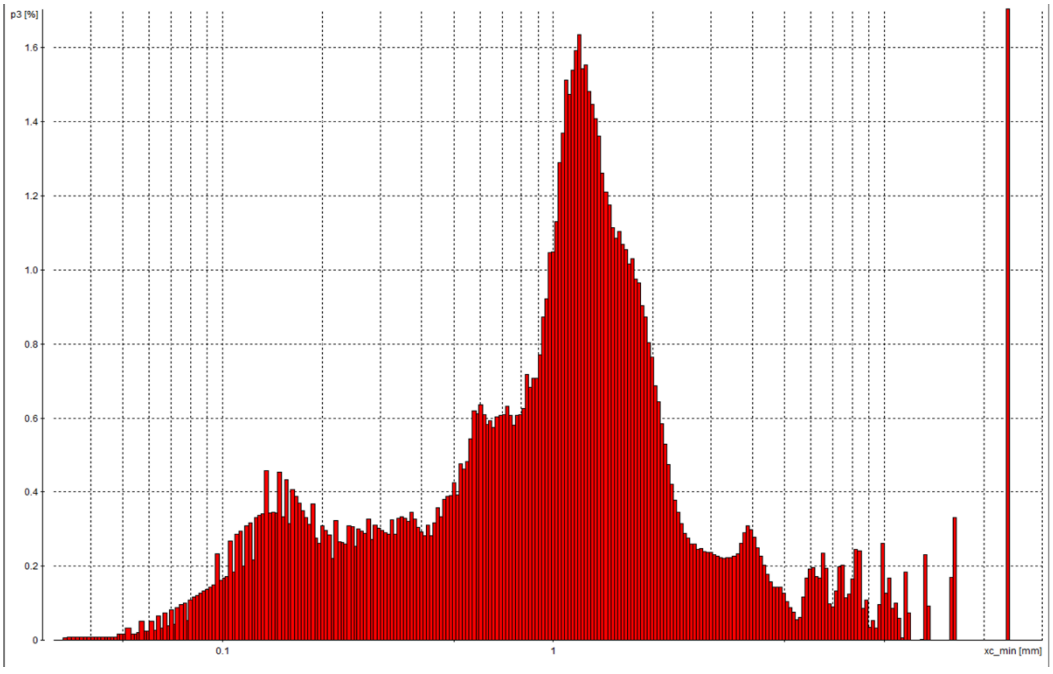

Figure 27. d50 of 0.784mm / Cu of 6.75 Camsizer Distribution

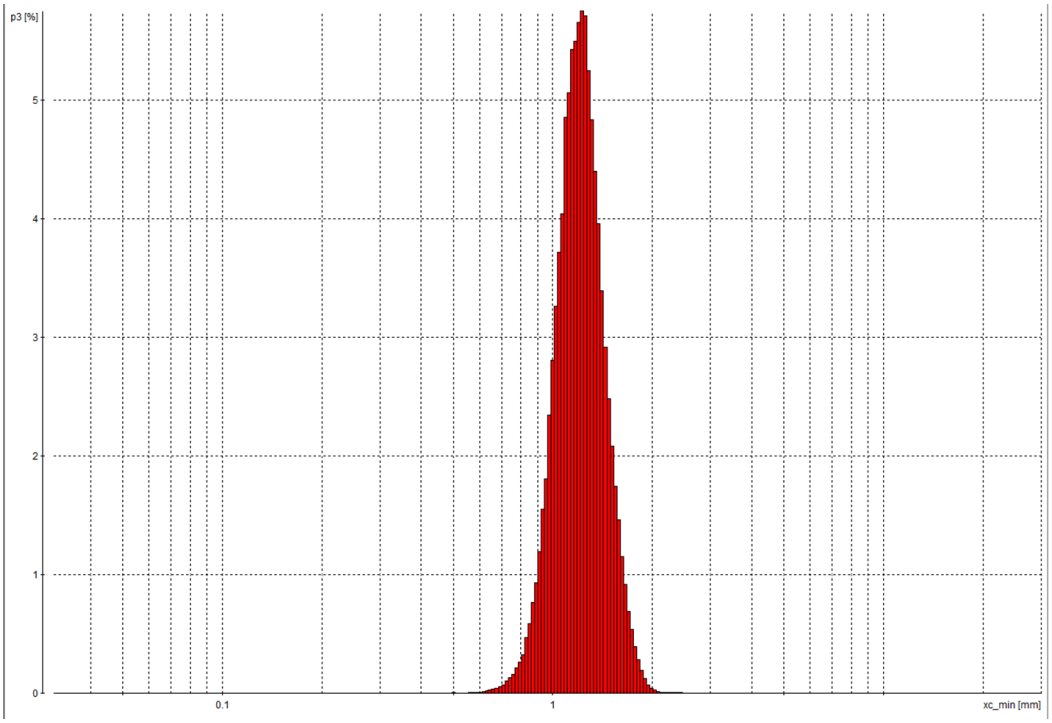

Figure 28. d50 of 1.093mm / Cu of 1.5 Camsizer Distribution

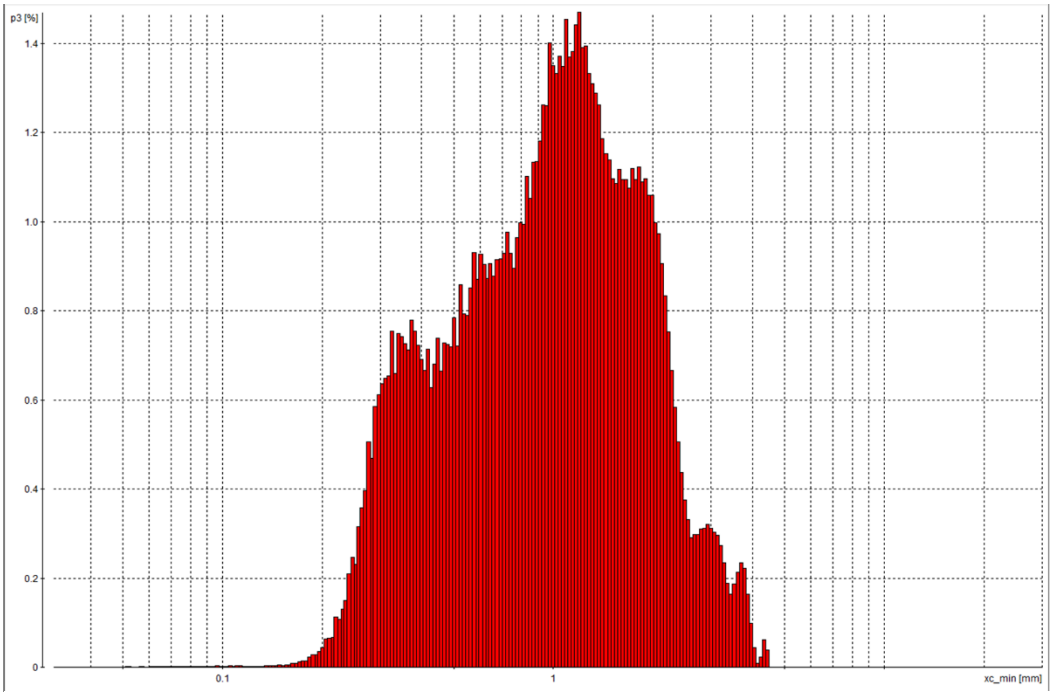

Figure 29. d50 of 0.994mm / Cu of 3.3 Camsizer Distribution

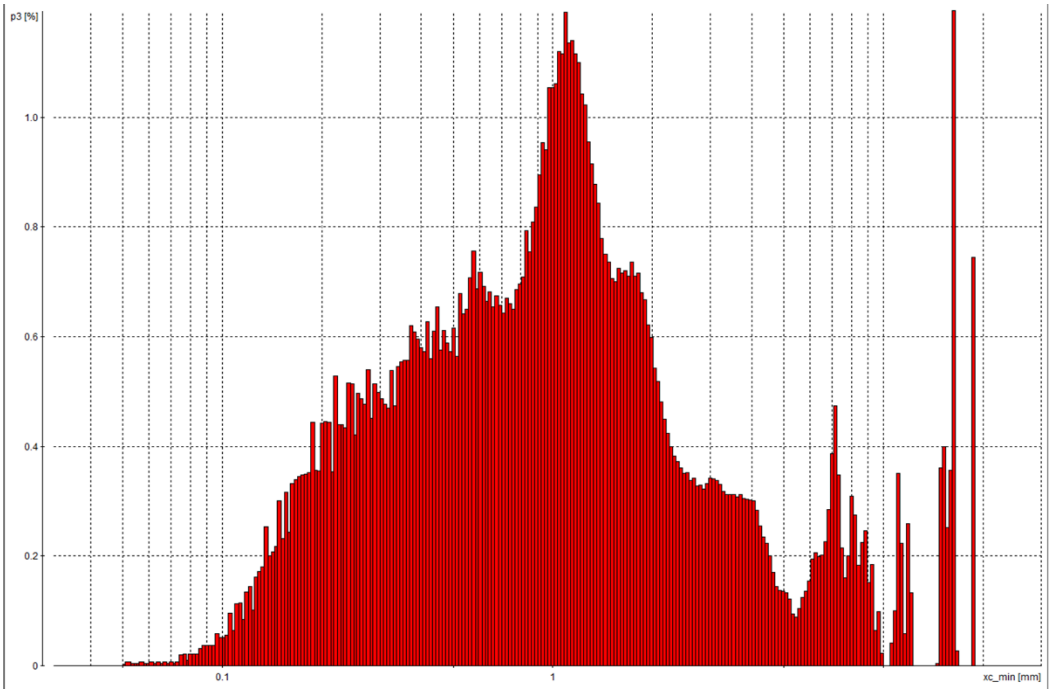

Figure 30. d50 of 0.990mm / Cu of 6.25 Camsizer Distribution

Appendix B

Below are the results of the failure rate calculations. Failure rate is found via taking the slope of the decrease in gradient during piping failure.

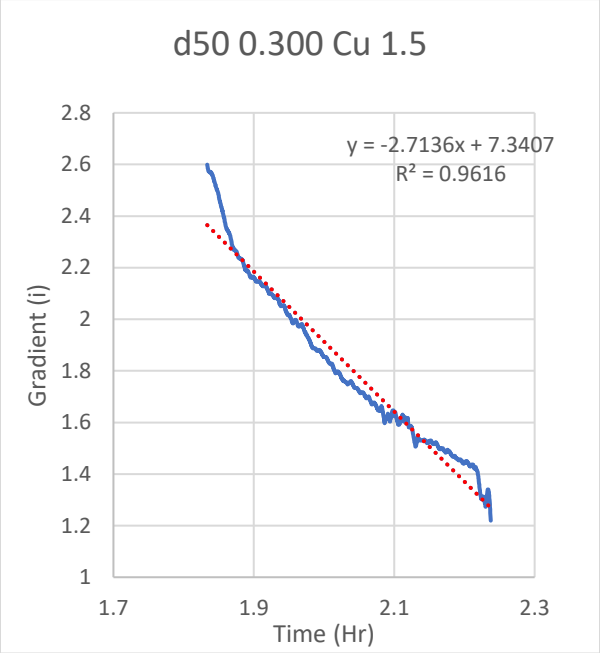

Figure 31. d50 of 0.300mm / Cu of 1.5 Fail Rate

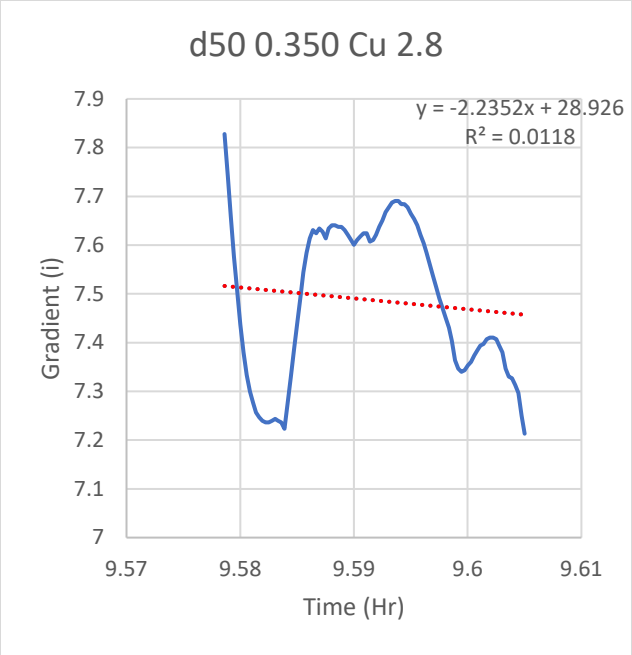

Figure 32. d50 of 00.350mm / Cu of 2.8 Fail Rate

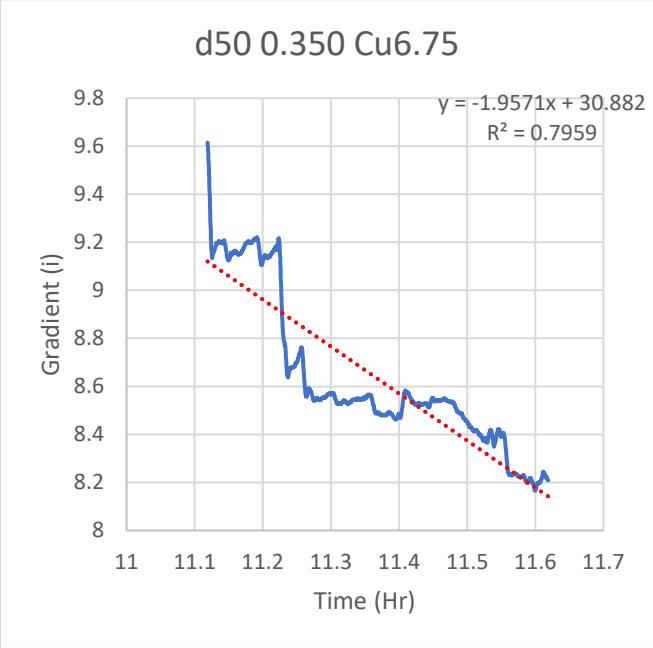

Figure 33. d50 of 0.350mm / Cu of 6.75 Fail Rate

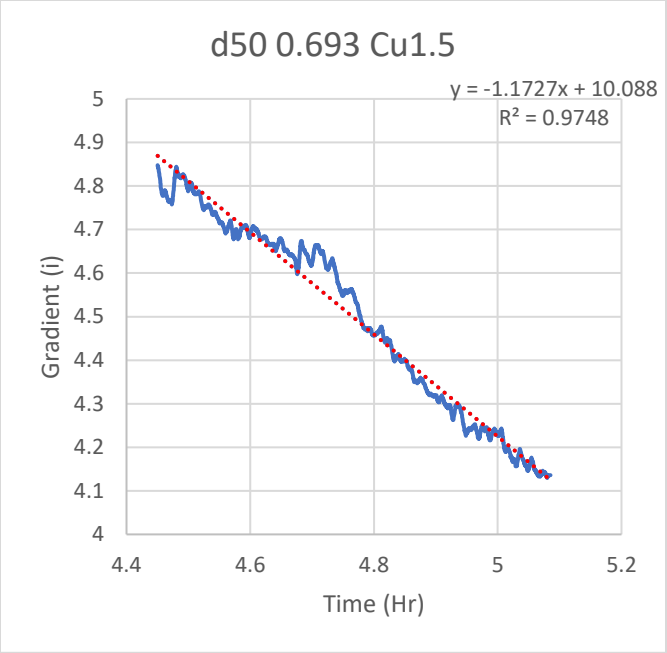

Figure 34. d50 of 0.693mm / Cu of 1.5 Fail Rate

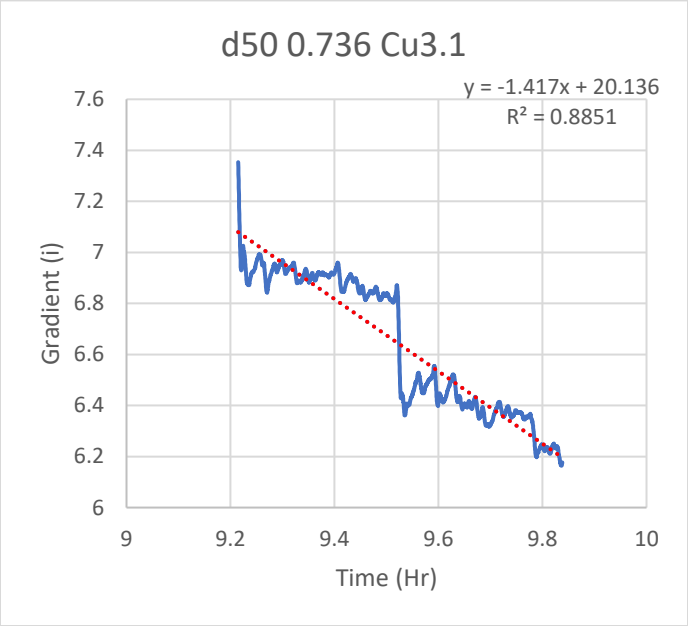

Figure 35. d50 of 0.736mm / Cu of 3.1 Fail Rate

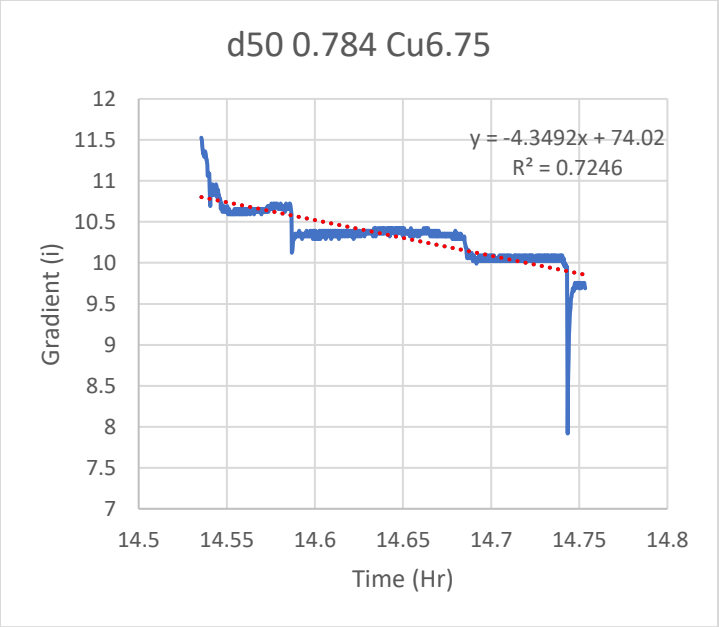

Figure 36. d50 of 0.784mm / Cu of 6.75 Fail Rate

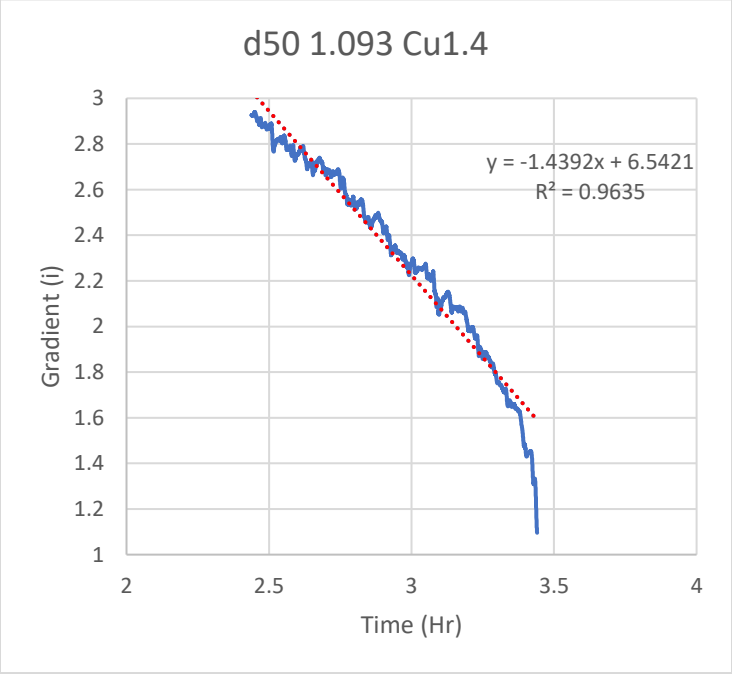

Figure 37. d50 of 1.093mm / Cu of 1.4 Fail Rate

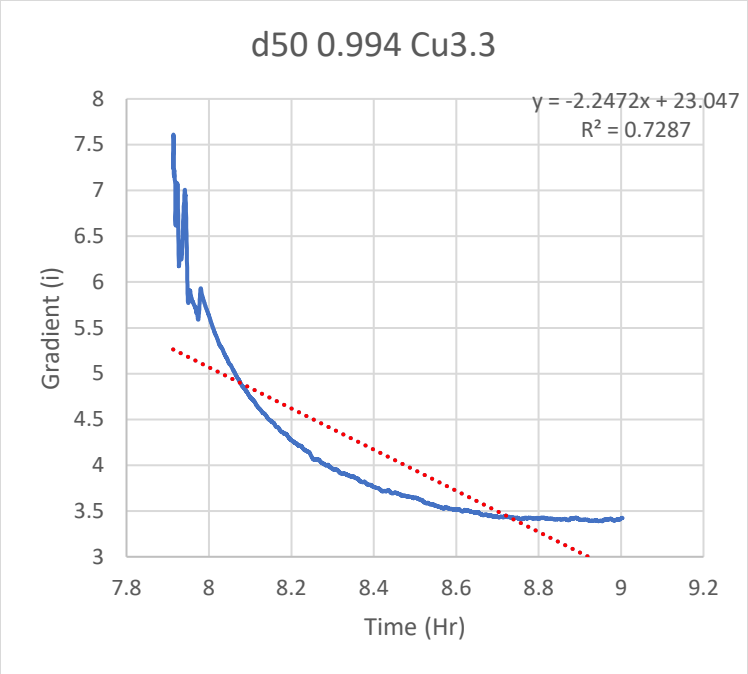

Figure 38. d50 of 0.994mm / Cu of 3.3 Fail Rate

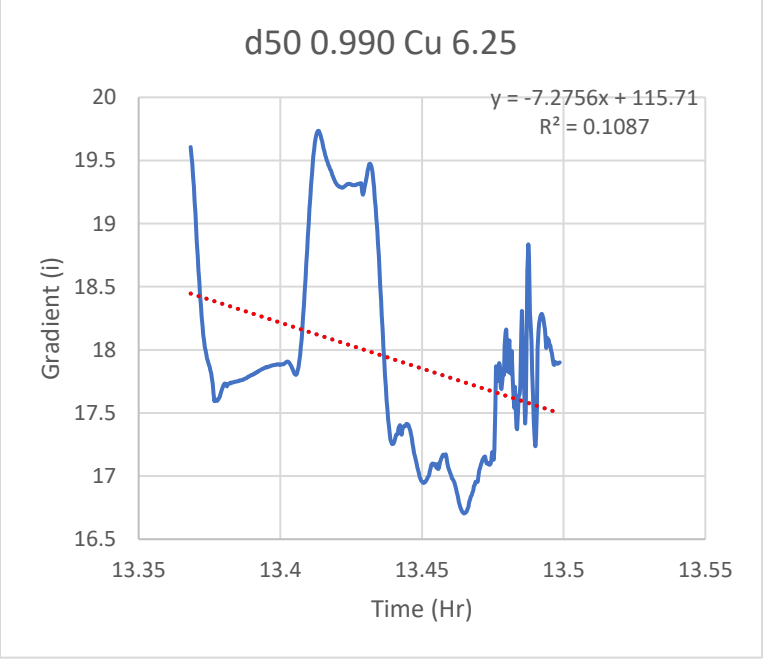

Figure 39. d50 of 0.990mm / Cu of 6.25 Fail Rate